Title

Mineralogic controls on the infrared stimulated luminescence of feldspars: an exploratory study of the effects of Al,Si order and composition on the behavior of a modified post-IR IRSL signal

Author

Daniels, JILLIAN

Publication Date

2016

UNIVERSITY OF CALIFORNIA

Los Angeles

Mineralogic controls on the infrared stimulated luminescence of feldspars: an exploratory study of the effects of Al,Si order and composition on the behavior of a modified post-IR IRSL signal

A thesis submitted in partial satisfaction

of the requirements for the degree Master of Science

in Geology

by

JILLIAN THERESA Daniels

2016

ABSTRACT OF THE THESIS

Mineralogic controls on the infrared stimulated luminescence of feldspars: an exploratory study of the effects of Al,Si order and composition on the behavior of a modified post-IR IRSL signal

by

JILLIAN THERESA Daniels

Master of Science in Geology

University of California, Los Angeles, 2016

Professor Kevin D McKeegan, Chair

The luminescence characteristics of a variety of feldspars were investigated using the post-IR IRSL signal to facilitate the understanding of the origins and behavior of signals used in luminescence dating. These feldspars were characterized in terms of major composition, Al,Si ordering, and minor impurities, and compared to the luminescence decay parameters of brightness, bleachability, and kinetic order calculated from the pIRIR decay signal. The behavior of these parameters over varying preheat temperatures, pIRIR measurement temperatures, IR50 measurement times, and first IR measurement temperatures were analyzed. Correlations between the physical and the luminescence characteristics were noted, as well as the general behavior of similar feldspar samples over different dating protocol parameters. Variations in Al,Si order were found to have the largest effect on K-feldspars, although some luminescence parameters were surprisingly insensitive. It may be that <*T*-O> bond length has a fundamental effect on the luminescence origin of all feldspar species.

Supplementary materials are spreadsheets of the XRD calculated unit cell parameters of each sample, the calculated luminescence parameters of the pIRIR decay for experiment 1 (varying preheat temperature), experiment 2 (varying pIRIR temperature), experiment 3 (varying IR50 time), and experiment 4 (varying first IR measurement temperature). Spreadsheets of the calculated luminescence parameters of the IR50 decay are also included for experiment 1 (varying preheat temperature) and experiment 3 (varying IR50 time).

The thesis of JILLIAN THERESA Daniels is approved.

Edwin Arthur Schauble

Edward Rhodes

Craig E Manning

Kevin D McKeegan, Committee Chair

University of California, Los Angeles

2016

DEDICATION

This thesis is dedicated to Ryan Caron.

Without you, none of this would have been possible.

Table of Contents

List of Equations

List of Figures

Acknowledgements

Funding for this research was supported in part by the grants "Collaborative Research: Interaction Between Holocene Lake Levels and Alluvial Fans in the Western U.S. in Response to Changing Climates" (NSF Geomorphology, award #EAR-1251690) and "Collaborative Research: Extending the Record of Incremental Slip Rate Variation on the Central Garlock Fault throughout the Holocene Using Newly Developed Luminescence Sediment Dating" (SCEC/USGS, award #57266713)".

Culver City Rock & Mineral Club kindly provided use of their lapidary shop and jewelry saw.

Michael Lawson assisted in the drafting of Figure 1.

Ryan Caron provided formatting services and general moral support for this thesis.

1. Introduction

Optically stimulated luminescence (OSL) is a dating method used in many geologic and archaeologic contexts. Over time, background radiation causes a buildup of trapped charge in buried mineral grains. This buildup is released by certain zeroing events, such as exposure to light (called “bleaching”) or heat. The absorbed dose of a grain can be measured by shining stimulating light on it (usually from a laser or LED source) and measuring the resulting luminescence (filtering out the stimulation wavelengths). The growth of this signal in response to a controlled dose of radiation gives information on the sensitivity of a sample. Combining this information with the rate of background radiation at the sample collection site, the elapsed time since the last zeroing event (“age”) can be calculated (Rhodes, 2011).

Infrared stimulated luminescence (IRSL), a subset of OSL, is generally used for dating in feldspar grains. Alkali and specifically K-rich feldspars are preferred as grains with these compositions seem to have luminescence properties more easily exploited to accurately determine the absorbed dose. A new method, post-IR IRSL (pIRIR), uses the signal of a second IRSL measurement taken at a higher temperature immediately after the first. This signal appears to suffer less from anomalous fading, the apparent “leaking out” of trapped charge via quantum mechanical tunneling, which can lead to age underestimation (Buylaert et al., 2009). The pIRIR method is still being refined and developed.

Despite recent developments in our understanding of the origins of luminescence in feldspars, such as Jain and Ankjærgaard (2011), we still do not have a complete understanding of which characteristics control a feldspar’s suitability for IRSL analysis in general and post-IR IR dating in particular. In addition, the details of the physical model of the luminescence generating process for feldspars in general are still not clear, although dependence of the IRSL signal on the distance within the crystal lattice between

electron trap and luminescence center (hole trap) appears important (Jain & Ankjærgaard, 2011; Jain et al., 2015). This theoretical model is discussed further in Section 2.2.

The word “feldspar” refers to a wide variety of minerals, and even the common varieties may vary considerably in physical and mineralogical properties. Comprehensive studies comparing luminescence to physical or chemical characteristics for feldspars are relatively rare and usually concentrate on K-Na-Ca ratios (such as Tsukamoto et al., 2011), and most predate the introduction of pIRIR methods (Spooner, 1994; Duller, 1997; Krbetschek et al., 1997). Most of the recent work on the pIRIR signal concentrates on evaluating the validity of ages calculated using this method, using grains extracted from sediments (such as Smedley et al., 2015), which may be sourced from several different parent rocks with widely varying characteristics. Few studies analyze and discuss the effects of differing Al,Si ordering, except in the broadest of terms. Generally, when feldspars with a variety of physical and chemical characteristics are specifically sought out by luminescence researchers, it is to evaluate aspects of IRSL behavior common to all feldspars, instead of to analyze the differences.

The distinction between feldspars of different composition and Al,Si ordering is not often emphasized in luminescence research except in the broadest of terms, perhaps because many luminescence researchers have backgrounds in physics rather than geology or mineralogy and are not so widely exposed to the variation within this group of minerals. Some early papers in the 1980s only referred to their specimens as “feldspar”, neglecting to make a distinction even between alkali feldspars and plagioclase. When the term “orthoclase” is used, it is not always clear whether the authors are referring specifically to a potassic feldspar with intermediate Al,Si disorder, or just using the term as a shorthand for any K-feldspar. More worryingly, one of three cornerstone samples used to represent the three compositional endmembers of feldspar in the first paper to propose a comprehensive model of feldspar luminescence may have been gravely mischaracterized. Morthekai et al. (2013), using some of the same

samples as the seminal Jain and Ankjaergaard (2011), performed compositional analysis using inductively coupled plasma optical emission spectrometry (ICP-OES). They note that the sample Jain and Ankjaergaard used to represent the sodic endmember albite actually has a composition of Ks_{78}, and call it “sanidine1”. Sample 010 sanidine used in this research was often found to have behavior noticeably distinct from other K-feldspars, and is far different, probably on a fundamental level, from the most albitic sample, 011 Na-plagioclase (An_{31}). Though there is no mention of how Morthekai et al. determined the Al,Si ordering of the “sanidine1” sample, if this assertion is not a typo and Jain and Ankjærgaard did mistake a sanidine for an albite in their 2011 paper, this error may have had negative repercussions on the accuracy of our current understanding of how luminescence characteristics change with composition, and is symptomatic of the poor treatment of feldspar mineralogy in the community as a whole.

This exploratory study used a suite of feldspar samples covering a wide range of compositions and Al,Si ordering. These characteristics were analyzed and confirmed using a scanning electron microscope (SEM) and an X-ray powder diffractometer (XRD). Several amazonite samples (an unusual green-blue Pb-bearing type of microcline) were included to investigate the effects of minor compositional components. A Risø OSL reader was used to measure the luminescence decay while systematically varying the dating protocol parameters of preheat temperature, pIRIR measurement temperature, first IR measurement time, and first IR measurement temperature. Analysis concentrated on the pIRIR signal. Software was coded in the programming language MATLAB in order to fit the observed luminescence signals to a modified version of the decay equation suggested by Bailiff and Barnett (1994) and calculate the luminescence decay characteristics related to sensitivity, bleachability, background decay, and kinetic order, discussed further in Section 4.4. MATLAB was also used to assist in analyzing patterns and

correlations between the physical and the luminescence characteristics, as well as the general behavior of similar feldspar samples over different dating protocol parameters.

While this research represents a broad exploratory study, and any conclusions should be confirmed with more targeted experiments, these questions were kept in mind: do systematic differences in major composition, Al,Si ordering, or presence of certain minor impurities have any correlations with luminescence characteristics in feldspars? If so, what are the implications about the fundamental origin of the luminescence signals? Are there certain parameters of the standard pIRIR dating protocol that may be varied in order to recover a reliable signal in feldspars unsuitable for dating using current methods?

2. Background Information

2.1. Mineralogy of feldspars

Feldspars are the most abundant minerals in the Earth's crust. Their modal percentages are used in the classification of igneous rocks, as they are absent only from some ultrabasic and rare alkaline igneous rocks (Le Bas & Streckeisen, 1991). Feldspars are found in most metamorphic rocks. In arenaceous sediments, they are the second most abundant minerals after quartz. They are of relatively minor importance only in the argillaceous and carbonate sedimentary rocks. Around two thirds of the Earth's exposed continental rocks have a significant quantity of feldspar (Deer, Howie, & Zussman, 2001; Amiotte Suchet et al., 2003).

A review of 12 studies of the feldspar content of sands, including 404 samples of recent-to-Pleistocene North American sands, gives an average of 15.3% feldspar by volume. Of those studies that gave ranges

of their individual samples, the range was 1 to 77%. River sands had more feldspar at 22%, while beach sands averaged 10.1% and dune sands 10.6% (Pettijohn, Potter, & Siever, 1987). Since an abundance of only a few percent is needed to get a good yield of feldspars for luminescence dating (Rhodes, 2016, personal communication), one could assume that the vast majority of sands available for sampling have sufficient feldspar content. Note that there may be locations with feldspar samples that are not well-suited for IRSL dating, the primary focus of this research. However, a detailed survey of this lies beyond the scope of this research.

Feldspar composition can be visualized as a ternary, measured in mol%, with endmembers $CaAl_2Si_2O_8$ (anorthite, or An), $NaAlSi_3O_8$ (albite, or Ab), and $KAlSi_3O_8$ (see Figure 1). While K-rich feldspars are often all referred to as "orthoclase" and abbreviated as Or, this term properly refers to a specific structural variety of potassium-rich feldspar with an intermediate degree of Al,Si ordering. This thesis instead will use the word "K-feldspar" and abbreviation Ks after Nesse (2012). Feldspars with compositions between Ks and Ab are referred to as the alkali feldspars, and those ranging from Ab to An are called plagioclase feldspars.

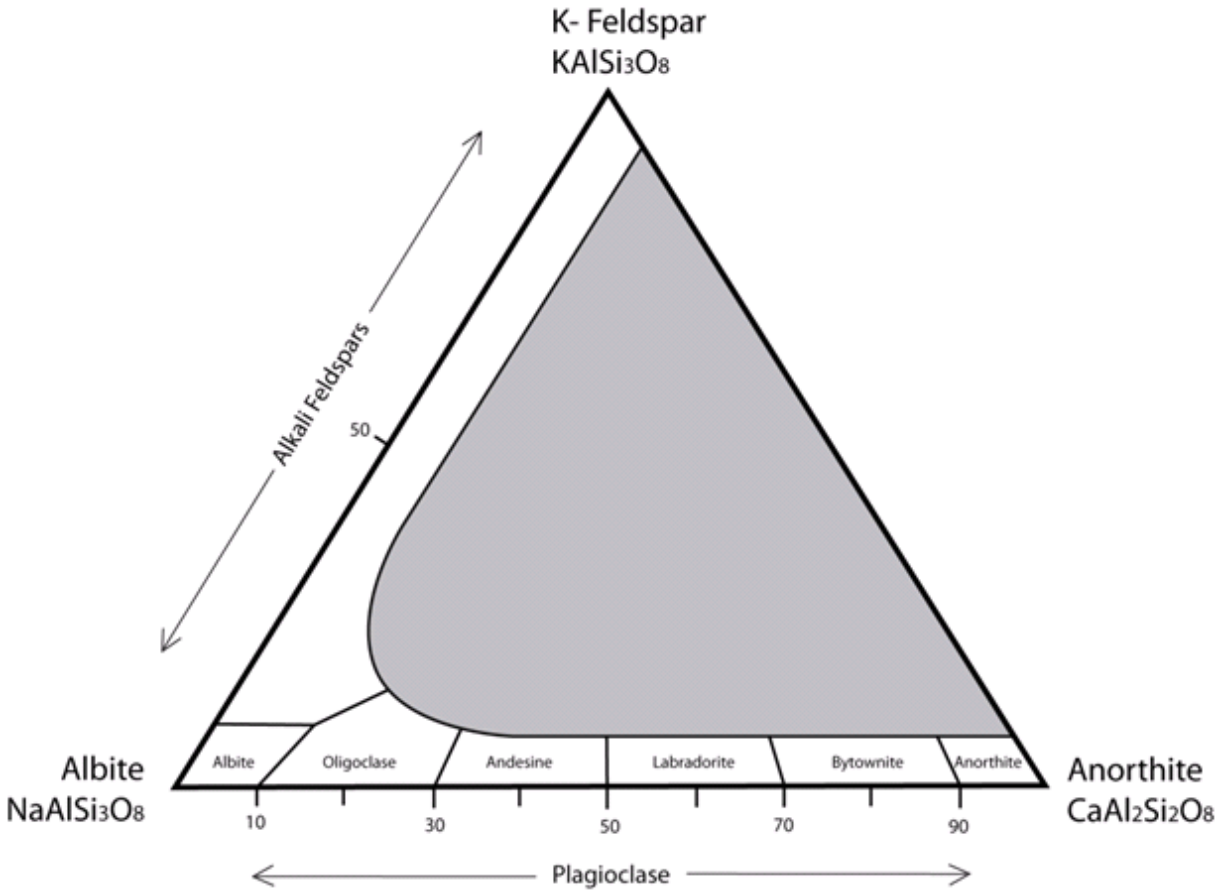

Figure 1 Ternary diagram of the feldspar minerals

In the alkali feldspars, four tetrahedral sites in the crystal structure hold one Al^{3+} and three Si^{4+} ions. The distribution of these ions determines the Al,Si ordering and thus species name. K-feldspars with a high degree of order are microcline, those with a low degree of order are sanidine, and those in the middle are orthoclase (Deer, Howie, & Zussman, 2001). A more detailed discussion of Al,Si ordering and its consequences can be found in Section 2.1.2.

While this is a review of the properties of both alkali and plagioclase feldspars, this study focuses on the alkali and specifically K-feldspars, and this review will reflect that.

2.1.1. Major composition: K, Na, Ca

Most feldspars fall on the aforementioned anorthite-albite-K-feldspar ternary. Only compositions between An – Ab and Ab – Ks are found. The lack of allowable compositions between Ks – An, under any geological conditions, is because K^+ and Ca^{2+} differ in both charge and size (Nesse, 2012). Generally there is less than K_{5-10} in the plagioclases and An_{5-10} in the alkali feldspars, though there can be somewhat more in the compositions near end-member albite. At this part of the ternary the distinction between plagioclase and alkali feldspars is somewhat arbitrary, and Deer, Howie, and Zussman (2001) suggest a practical boundary where K = Ca (see Figure 1).

There is continuous solid solution in the alkali feldspar series at high temperatures because K^+ and Na^+ have the same charge. However, there is a miscibility gap at lower temperatures because of the difference in ion size; Na^+ has an effective radius of around 1 Å, while K+ is around 1.3 Å. This gap in solid solution widens with decreasing temperature. At surface conditions solid solution between Ab and Ks occurs only at Ks_{95-100} at the potassic end and barely at all on the sodic end (Smith & Brown, 1988; Nesse, 2012; Ribbe, 1983; Deer, Howie, & Zussman, 2001).

Over time, alkali feldspars with bulk compositions falling within the miscibility gap slowly unmix, with the exsolved albite forming Na-rich exsolution lamellae. This intergrowth texture is sometimes called perthite. When K-feldspar is exsolved out of an Na-rich host, it is termed antiperthite. These structures can range from submicroscopic to stringers several mm thick, and are often found on several different scales in the same grain (see Figure 2). The size and morphology of these features is controlled by the composition and thermal history, among other factors. In general, the slower the crystal cooled, the larger the perthite texture will be, although interaction with water also seems to play a role. Exsolution lamellae visible to the naked eye are often found in microclines. In sanidines they are usually

microscopic (microperthite) to submicroscopic (cryptoperthite) (Nesse, 2012; Deer, Howie, & Zussman, 2001). Only the most quickly quenched K-feldspars, such as ashfall sanidine, may lack this structure completely (Martin, 2014, personal communication).

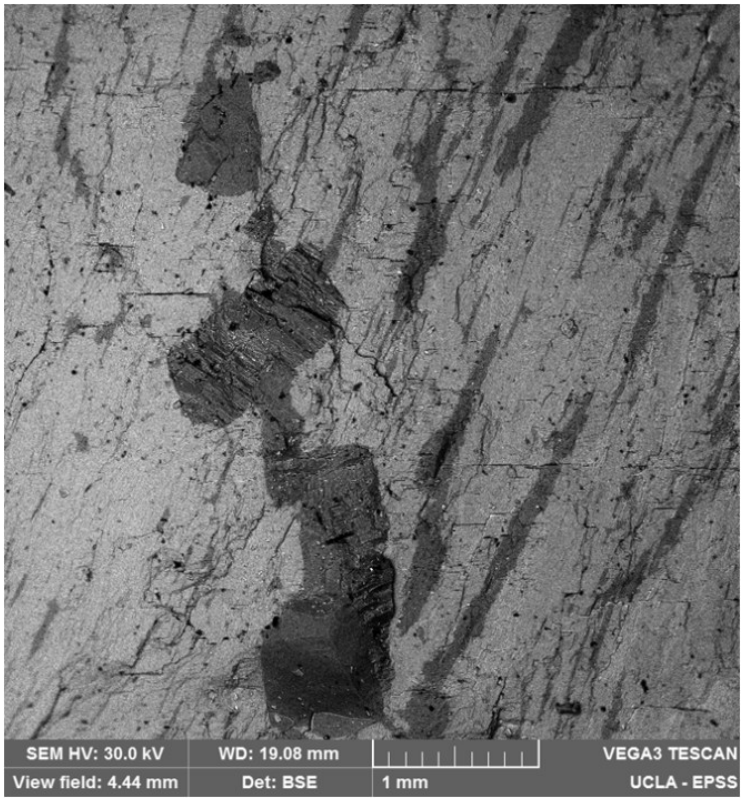

Figure 2 Exsolution lamellae of a K-feldspar. imaged using a scanning electron microscope. Note the different scales.

Plagioclase has continuous solid solution at high temperatures between calcic An and sodic Ab, because Ca^{2+} and Na^{+} are approximately the same size. One Al^{3+} substitutes for an Si^{4+} to offset the extra charge introduced by the Ca^{2+} ion. However, there are three miscibility gaps at low temperature, caused not by differences in ionic radii but incompatibilities in Al,Si ordering from albite to anorthite. Low temperature crystals with bulk compositions falling in these gaps exhibit specific types of intergrowths, called 'e' structures. While these lamellae are often submicroscopic, the thickness may be around the same as the wavelength of light and thus act as a diffraction grating, causing the visual properties known variously as

iridescence, labradorescence, or schiller. The most common naming convention for plagioclases relies only on composition: An_{0-10} is albite, An_{10-30} oligoclase, An_{30-50} andesine, An_{50-70} labradorite, An_{70-90} bytownite, and An_{90-100} anorthite (see Figure 1). These ranges are chosen for convenience and have no structural significance (Nesse, 2012; Deer, Howie, & Zussman, 2001).

Density varies in the feldspars mostly in response to composition. The specific gravity of anorthite is 2.76. Su et al. (1986) showed that for the alkali feldspars, specific gravity varies inversely with Ks content, decreasing from 2.62 at Ks_0 (albite) to 2.56 at Ks_{60} (wt%) after which it seems to level out. Disordered alkali feldspars were found to be slightly less dense than their ordered counterparts when the Ks content was less than 60 wt%, but above that composition the difference was negligible.

Density separation is often used during sediment preparation for IRSL dating to separate the K-feldspar grains from other minerals not removed by other means, most commonly quartz and plagioclase. This is discussed further in Section 4.4.

2.1.2. Al,Si ordering

Feldspars, along with quartz, zeolites, feldspathoids such as leucite, and some other minerals such as analcime, are tectosilicates. Also known as framework silicates, the crystal structure these minerals is based on a framework of TO_4 tetrahedra: each tetrahedral *T* site is coordinated with four oxygen anions. Each oxygen ion is shared with another tetrahedron, reducing the relative abundance of oxygen ions, and the generalized formula is TO_2. In quartz, all *T* sites are occupied by Si^{4+} ions, and the structure is electrically neutral. In the feldspars, one or two out of every four *T* sites is occupied by Al^{3+} instead; other cations must be added to balance the net negative charge (Nesse, 2012).

Thus, when attempting to visualize their crystal structure, it is helpful to generalize the feldspar formula to AT_4O_8. These tetrahedra form four-member rings, with the apices of two of them pointing up along the *a*-axis and two pointing down. The tetrahedra in these rings share corners with tetrahedra in other rings to form a crankshaft-like structure parallel to the *a*-axis. These chains are joined laterally to other chains by sharing their remaining corners, forming the framework of the crystal structure and creating the *A* sites that can hold large cations such as Ca^{2+}, Na^{+}, and K^{+}. (Ribbe, 1983; Nesse, 2012)

In alkali feldspars, the four tetrahedral sites are designated T_1o, T_1m, T_2o, and T_2m. (For plagioclase the nomenclature is similar but involves complications outside the scope of this thesis.) In the triclinic feldspars T_1o and T_1m are related by pseudo-mirror planes parallel to (010). For the monoclinic feldspars, it is a true mirror plane; T_1o and T_1m are equivalent and referred to collectively as T_1. The same goes for T_2o and T_2m (Ribbe, 1983).

In monoclinic feldspars, t_1 represents the (average) Al content of the T_1 site. Since each four-member ring of tetrahedra contains three Si^{4+} and one Al^{3+} ion, we may write

$$2t_1 + 2t_2 = 1.0$$

Equation 1

If the distribution is random, the feldspar is said to be completely disordered:

$$t_1 = t_2 = 0.25 \text{ or } 2t_1 = 2t_2 = 0.5$$

Equation 2

In the K-feldspars, Ribbe (1983) suggests the values $2t_1 = 0.5 – 0.667$ for high sanidine, $2t_1 = 0.667 – 0.75$ for low sanidine, and $2t_1 = 0.75 – 1$ for orthoclase, though these limits are only guidelines. Thus the most

ordered orthoclases have the Al^{3+} ions strictly found in the T_1 sites. The T_1 sites are preferred to T_2 by the Al^{3+} ions because the oxygen ions coordinating T_1 are more closely bonded to the large A^+ cation than those of T_2.

To achieve higher Al,Si order, t_1o and t_1m must no longer be equivalent, destroying the (010) mirror plane and thus degenerating the symmetry from monoclinic to triclinic. A fully ordered microcline (also termed low or maximum microcline) is thus represented by:

$$t_1o = 1.0; t_2m = t_2o = t_2m = 0$$

Equation 3

Triclinic K-feldspars with an intermediate degree of order are called intermediate microcline and generally follow the formula:

$$t_1o > t_1m > t_2o = t_2m$$

Equation 4

remembering that

$$t_1o + t_1m + t_2o + t_2m = 1.0$$

Equation 5

Ordering is achieved by the Al^{3+} ions diffusing through the crystal lattice. Thus K-feldspars with higher formation temperatures and faster cooling times tend to have greater disorder – for example, volcanic K-feldspars tend to be sanidine, while plutonic crystals are usually orthoclase and microcline. Pressure and water content also play a role (Deer, Howie, & Zussman 2001).

In Na-feldspars, near-complete ordering akin to maximum microcline (Equation 3) is exhibited by low albite, whereas high albite is the analogue of intermediate microcline (Equation 4). The sodic equivalent of sanidine (Equation 2) is called analbite. While its Al distribution is topochemically monoclinic, analbite is topologically (geometrically) triclinic; unlike K^+, the highly anisotropic Na^+ ion is too small to keep the *A* site "propped open" below ~980°C. The tetrahedral framework collapses slightly and the unit cell distorts into triclinic symmetry. Above ~980°C thermal vibration is sufficient to maintain monoclinic symmetry and analbite inverts to monalbite. Analbite is not generally found in nature (Ribbe, 1983; Nesse, 2012).

In the calcic plagioclase endmember anorthite, there are two Si^{4+} and two Al^{3+} ions. Here full ordering is defined as when Al and Si alternate with strict regularity throughout the structure, per the aluminum avoidance principle. Since the Al content varies along with the Ca content for charge balancing across the plagioclase range (one way to think of the chemical formula is $(NaSi, CaAl)AlSi_2O_8$), feldspars in the range $An_{\sim 25\text{-}85}$ are actually blocks of intergrown lamellae with alternating "albite-like" and "anorthite-like" structures, known as 'e' plagioclases. All plagioclases are triclinic at surface temperatures and pressures (Deer, Howie, & Zussman, 2001).

2.1.2.1. *T*-O bond length

The average length of the bond between a tetrahedral Al^{3+} and its four oxygen ions, <Al-O>, is about 0.13 Å, longer than <Si-O>. Thus the average bond length for all tetrahedral-oxygen bonds, <<*T*-O>>, increases from 1.64 Å for albite to 1.68 Å for anorthite – the amount of aluminum is doubling, after all. However, the ordering and thus distribution of Al^{3+} is important as well: an individual Si-O bond will be around 0.03 Å longer if the oxygen ion is bonded to another Si^{4+} compared to Al^{3+}. A microcline and

sanidine may have similar <<*T*-O>>, but the disordered sanidine will have a broader distribution of individual *T*-O lengths. The coordination number of the oxygen ion to the *A* cation (which changes between K^+, Na^+, and Ca^{2+}) also has an effect on *T*-O bond distances. *T*-O-*T* bond angles and unit cell parameters change due to differences in *T*-O bond length; this fact is taken advantage of by Kroll and Ribbe (1983) in order to calculate Al,Si ordering using XRD analysis, discussed further in Section 4.3.

The results of this research suggest T-O bond length average and distribution may play a significant, even fundamental role in the origin and character of the luminescence signals, not just for feldspar, but also quartz and certain feldspathoids such as leucite – see further discussion in Section 6.

2.1.2.2. Optical and physical properties

There are distinct differences in the optical and physical properties between sanidine, orthoclase, and microcline; after all, they were originally distinguished and named in the early 1800s using characteristics observable with the naked eye, such as crystal habit, fracture, and geologic context. Further refinements of their definitions were made using petrographic microscopes, prior to the invention of technology that would allow the determination of their chemical structures. Two of the three indices of refraction vary linearly with $t_1o + t_1m$, which in turn influence optical properties derived from these parameters, such as optic plane orientation and $2V_x$ angle (Nesse, 2012).

The change in unit cell with Al,Si order brings with it a change in symmetry, which controls the shape in which crystals grow and the angles at which they fracture. Sanidine and orthoclase are monoclinic, while microcline is triclinic. The second least symmetric crystal system, the three length parameters of a monoclinic unit cell are of different lengths; and two of the cell angles are 90°, with the third being some other value. Triclinic crystals are the least symmetric; none of the three angles may be 90°. As microcline

has only a small relative distortion from a monoclinic structure, these disrupted cell angles are only slightly distorted (90.65° and 87.65°, hence the Greek name “micro-cline” – “small incline”) (Nesse, 2012).

This inversion of symmetry has another consequence. As a K-feldspar crystal undergoes progressive ordering, depending on which complement of T_1 sites happen to accumulate the Al^{3+} ions (and thus turn into T_1o sites), the triclinic structure can be related to the monoclinic structure in several equally likely orientations. Different areas of the crystal will orient in dissimilar ways, causing polysynthetic albite and pericline twinning, which can be observed as “tartan” or “gridiron” twinning. K-feldspar which crystallizes with low Al,Si disorder at a low temperature due to authigenic or hydrothermal processes is sometimes known as “adularia” and lacks this type of twinning (Nesse, 2012).

As mentioned in Section 2.1.1, Al,Si ordering may have a small effect on the density of sodic alkali feldspars.

2.1.3. Minor impurities: Ba, Sr, Rb, Pb, P, Fe, etc.

There are several minor ions that can substitute into the standard feldspar structure. In natural alkali feldspars, Fe^{3+}, Fe^{2+}, Mg, Ga, Ti, B, and P have been found substituting into the *T* sites, usually in small amounts, though sanidines with up to 70 mol% of their Ks ($KAlSi_3O_8$) content replaced by ferric $KFeSi_3O_8$ have been reported by Kuehner and Joswiak (1996). Ba, Sr, and Rb may also be major constituents occupying the *A*-site. The most common of these are the barium feldspars. While most alkali feldspar has some quantity of barium, it is only rarely a major constituent. A feldspar is considered a barium feldspar when its BaO content is greater than ~2%. Feldspars greater than 80% $BaAl_2Si_2O_8$ are called celsian; those with less are termed hyalophane. Generally Rb is present only as a trace element in alkali

feldspars, with the exception of some highly fractionated rare-element granitic pegmatites. Rubicline, ideal composition $RbAlSi_3O_8$, forms a solid solution series with microcline. Strontium varies widely in alkali feldspars in acid plutonic rocks, from 10 to 10^3 ppm. Melluso et al. (1996) reported a sanidine from a phonolite sample from Mt Vulture volcanic center in central Italy with 7.37 wt% SrO. While there are several other endmember feldspars not found on the standard ternary, most are either very rare in nature or only known from laboratory synthesis (Deer, Howie, & Zussman, 2001; Smith, 1983).

One K-feldspar variety of particular importance to this study is amazonite. Amazonite is most commonly described as a green to blue lead-bearing microcline. Others include orthoclase and even other feldspar compositions with similar green-blue colors in the definition of amazonite. The lead is likely accommodated into the feldspar structure by substituting (Pb^{2+} + Al^{3+}) for (K^+ + Si^{4+}), though (Pb^{2+} + □) for ($2K^+$) is also possible, leading to defect structure (Foord & Martin, 1979; Čech et al., 1971; Deer, Howie, & Zussman, 2001).

The relationship between lead content and color is still not well understood. Though there is a general correlation of Pb content to color and all amazonites have some Pb, not all K-feldspars with high Pb-content are amazonite, nor do all amazonites have particularly high Pb-content. A study by Stevenson and Martin (1986) found no amazonites with less than 1000 ppm Pb; the highest value was 2 wt% PbO. The majority of non-amazonitic K-feldspars have Pb contents ranging from 15-40 ppm (Deer, Howie, & Zussman, 2001). Hofmeister and Rossman (1985) suggest that structurally-bound H_2O is also required for the characteristic amazonite color to develop.

2.2. Stimulated luminescence in feldspars

2.2.1. Luminescence dating

Optically stimulated luminescence (OSL) is a type of luminescence dating used in geology, environmental sciences, archaeology, and anthropology. The basis of the technique takes advantage of trapped charge that builds up over time from background radiation in buried sediment grains, generally quartz or K-feldspar. This charge is depleted, or "bleached", by exposure to daylight, generally tens to hundreds of seconds in feldspar (Rhodes, 2011).

Dating mineral grains using this technique involves collecting them in such a way as to not accidentally expose them to light, which would destroy the built-up charge. The grains are stimulated with a laser or diode array and the resultant luminescence is measured. Generally this stimulation wavelength is around 870 nm for K-feldspar dating; hence Infra-Red Stimulated Luminescence (IRSL). Different samples, even of the same mineral, may build up charge at different rates, so their sensitivity is calculated by measuring the IRSL signal given off after being dosed with a controlled amount of radiation (Rhodes, 2011; Buylaert et al., 2012; Rhodes & Bailey, 1997).

These parameters are used to calculate equivalent dose, D_e, measured in the SI unit Grays (Gy; 1 Gy = 1 $J \cdot kg^{-1}$). The sample age is the equivalent dose divided by the background radiation measured at the collection site:

$$\text{age (years)} = \frac{D_e(\text{Gy})}{\text{dose rate (Gy year}^{-1})}$$

Equation 6

This gives the time elapsed since the sample was last bleached. 1σ uncertainties are typically on the order of ± 5 – 10% of the age of the sample (Rhodes, 2011).

The lower limit of measurable age depends on the luminescence properties of the sample, the background radiation rate experienced, and the sensitivity of the measuring equipment. Young samples can be measured with resolutions of several years, with some researchers believing it to be possible to measure time periods as short as months or even weeks (Rhodes, 2016, personal communication).

The upper age limit of datable events is limited by dose saturation; when all OSL electron traps are filled, no more trapped charge will result from additional radiation exposure. Quartz generally reaches this limit at around 200,000 years, although ages up to 350,000 years may be possible to measure in certain circumstances (Murray & Olley, 2002). K-feldspar IRSL signals tend to have a higher saturation limit, with the potential of dating sediments up to a million years, allowing for their application in much older contexts. Feldspar, like quartz, is ubiquitous in most geological contexts, but unlike quartz is often sensitive in tectonically active regions such as southern California (Lawson et al., 2015). However, an effect called anomalous fading can lead to age underestimation in certain older samples. It is thought that electrons quantum-mechanically tunnel their way to recombine with holes; effectively, some of the charge slowly "leaks out" (Wintle, 1973; Rhodes, 2011). Anomalous fading is further discussed in Section 2.2.2.

There are a few studies linking feldspar luminescence properties to composition, and it is generally agreed that K-feldspars have the best characteristics conducive to IRSL dating. Plagioclases, especially calcic plagioclases, tend to have weak signals (low sensitivity) and suffer from noticeably higher rates of anomalous fading. K-feldspars tend to be somewhat brighter than Na-feldspars. Having a lower density, they have the additional advantage of being more easily separated from quartz and plagioclase using a

centrifuge floatation separation technique. Studies linking Al,Si ordering are scarce, although it has been suggested that volcanic (thus likely disordered) K-feldspars have higher rates of anomalous fading (Spooner, 1992; 1993; 1994; Visocekas & Zink, 1995; Huntley & Lamothe, 2001).

2.2.2. Physical model

In quartz, background radiation causes bonding electrons to be excited from their valence positions, with a small fraction becoming trapped within the crystal lattice at energies between the valence and conduction bands (Rhodes, 2011). These electron and hole traps are thought to be formed at point defects in the quartz lattice, although the exact nature and structure is still under investigation (Martini et al., 2009; Itoh et al., 2002). Exposure to light excites the electrons, which are evicted from the traps and recombine with the holes at luminescence centers, giving off UV luminescence. The trap depth in quartz seems to be quantized to a limited number of values (Bailey, 2004).

While the electron model for luminescence in feldspars is thought to be similar to quartz, observed signals display significantly more complicated variations in behavior. Feldspars appear to have a much greater range and variation in the distribution of the depths of the electron traps. Poolton et al. (2002a; 2002b) suggested the role of band tail states: non-quantized trap states that are concentrated close to the band edges, tapering off in density deeper into the band gap. The complex thermal enhancement behavior of the feldspar IRSL signal (higher measurement temperatures tend to give brighter intensities) may arise from charge transport via “hopping” among the band-tail trap states. Jain & Ankjærgaard (2011) were the first to propose a comprehensive model of feldspar luminescence; they suggest that luminescence in feldspars arises from a single type of dosimetric trap, and it is the existence of the band-tail states that explain the complex range of observed thermoluminescence (TL) and thermal-

optical luminesce (IRSL) behavior in feldspars. Jain et al. (2015) further refines this model, concluding that the variation in thermal stabilities of different wavelength emissions results from differences in number densities of the recombination sites.

Poolton et al. (2002b) noted that band-tail states may arise from even slight impurities or deformation of the crystalline structure. Small variations in bond length may have large effects on the size of the band gap: Li and Ching (1985) calculated that in quartz, a variation of only 0.1 Å in the Si-O (*T*-O) bond changes the depth of the gap by 3.5 eV. Xu and Ching (1991) confirmed the link between bond length and energy gap.

The application of feldspar dating techniques has been hindered by anomalous fading (Wintle 1973; Spooner, 1992) in which electrons quantum-mechanically tunnel from their traps, giving anomalously younger equivalent doses (Jain & Ankjærgaard, 2011). Numerous methods have been proposed that would either characterize the nature of a sample's fading, allowing for a correction factor (Huntley & Lamothe, 2001; Auclair et al., 2003), or utilize a more stable signal that does not experience anomalous fading (Buylaert et al., 2009; Stokes & Fattahi, 2003). Thomsen et al. (2008) experimented with different stimulation and detection windows to find the combination that resulted in the least amount of fading within feldspar samples. From this work, Buylaert et al. (2009) developed the post IR-IRSL protocol (pIRIR), which reproduced the age calculation results from the standard IR dating measurements but with a much reduced fading correction (~39%). Post IR-IRSL has been successfully applied in several geologic contexts (Thiel et al., 2011; Brown et al., 2015).

2.2.3. Characteristics of IRSL decay curves

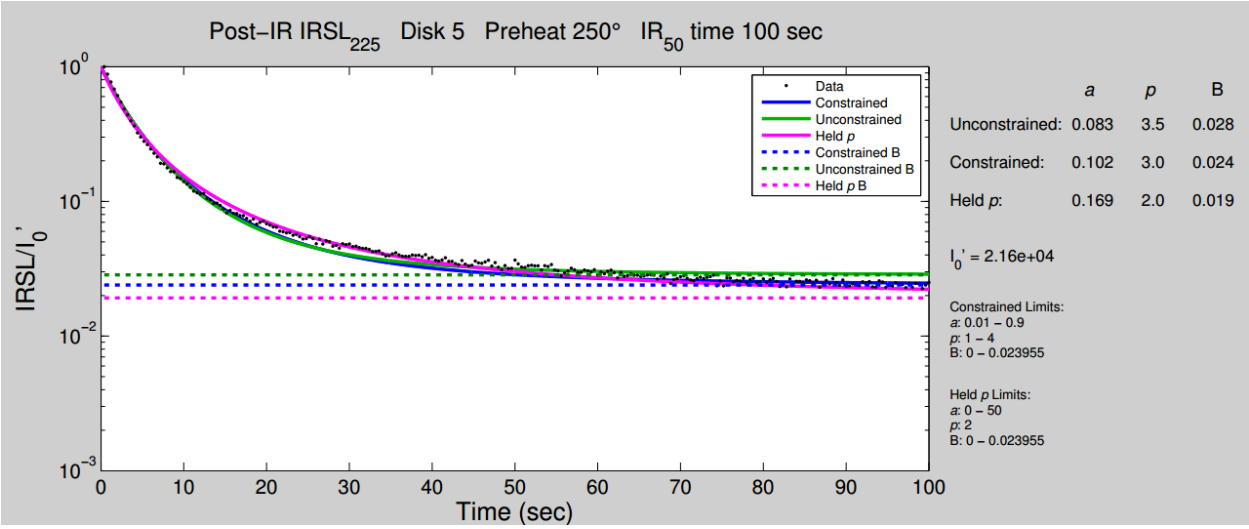

Figure 3 $pIRIR_{225}$ decay curve of sample 004 Papoose microcline made using the standard pIRIR measurement protocol.

Figure 3 displays a typical IRSL signal decay measured in this study. This measurement was made using a standard pIRIR measurement protocol as laid out in Section 4.4. The decay is reasonably well fitted using an equation set forth by Bailiff and Barnett (1994):

$$I = \frac{I_0}{(1 + at)^p} + R$$

Equation 7

This general form is encountered in most feldspar IRSL signals, and represents a fair approximation to the decay shape along with a convenient way to quantify the main characteristics of the curve by calculating the values of I_0, a, p, and R that allow the best fit of this formula to observed data. I is the brightness or intensity of the signal, with I_0 being the "initial intensity" at time $t = 0$. These are measured

in IRSL (photon) counts per second, although the formula is often normalized to I_0. Parameter *a* is sometimes called “bleachability” as higher values indicate a faster decaying signal. Parameter *p* is the order of decay of the equation. The constant R, called the residual, represents any component of the signal that decays slowly enough such that it would appear constant on the order of the measurement time. When the equation is not normalized to I_0, R also has units of IRSL counts per second.

The parameter *a* is not yet known to have clear physical significance, though it may be related to initial charge population, intensity of the excitation light, and capture cross section. It is in some ways similar to τ (lifetime) in an exponential decay. The ordering parameter *p* has also not yet been linked to a single physical characteristic of a given mineral species, although it is often interpreted as relating to the general kinetic order of the de-trapping process. It is generally held between 1 and 2 for feldspar luminescence decays (Bailiff & Barnett, 1994; Poolton et al., 2009; McGuire & Rhodes, 2015).

3. Sample Descriptions

The following sections describe the fifteen sample feldspars used in this study. Seven were collected in the field by the author from various locations in southern and eastern California, four were museum samples owned by the Earth, Planetary, and Space Sciences (EPSS) Department at UCLA, and four were purchased from mineral dealers.

Table 1 gives an overview of their physical characteristics; Table 2 gives details of their composition and Table 3 Al,Si ordering.

Sample	Name	Comp	t_1o	Group	Origin	Impurities
001	MJ40 labradorite	An_{67}	-	labradorites	museum	
002	San Gabriel labradorite	An_{68}	-	labradorites	San Gabriel Mts. (CA)	
003	Haystack amazonite	Ks_{94}	1.02	amazonites	Lone Pine, CA	Pb***
004	Papoose microcline	Ks_{84}	0.97	main K-feldspar group	Papoose Flat (CA)	
005	LGDH microcline	Ks_{90}	1.07	main K-feldspar group	San Gabriel Mts. (CA)	Ba
006	Pacoima microcline	Ks_{88}	1.01	main K-feldspar group	San Gabriel Mts. (CA)	
007	MJ39 interm. microcline	Ks_{88}	0.64	main K-feldspar group	museum	
008	Zion amazonite	Ks_{92}	0.96	amazonites	purchased	Pb***
009L	LGDP orthoclase light	Ks_{85}	* 0.42	main K-feldspar group	San Gabriel Mts. (CA)	Ba
009H	LGDP orthoclase heavy	Ks_{81}	* 0.42	main K-feldspar group	San Gabriel Mts. (CA)	Ba
010	sanidine	Ks_{87}	* 0.40	sanidine	museum	P
011	Na-plagioclase	An_{31}	-	Na-plagioclase	museum	
012	Brazil amazonite	Ks_{91}	** 1.11	amazonites	purchased	Pb***
013	Ethiopia amazonite	Ks_{95}	0.88	amazonites	purchased	Pb***
014	Russia amazonite	Ks_{92}	1.01	amazonites	purchased	Pb***

*monoclinic t_1o ***assumed

**likely measurement error

Table 1

Sample	Name	Comp.	Na	K	Ca	Lamellae Comp.	Na	K	Ca
001	MJ40 labradorite	An_{67}	33.20	0.62	66.19	-	-	-	-
002	San Gabriel labradorite	An_{68}	31.65	0.29	68.06	-	-	-	-
003	Haystack amazonite	Ks_{94}	5.58	84.84	9.58	Ks_{9}	90.13	8.39	1.48
004	Papoose microcline	Ks_{84}	16.03	81.88	2.09	Ks_{7}	90.19	6.35	3.46
005	LGDH microcline	Ks_{90}	9.44	81.24	9.32	Ks_{7}	87.34	6.86	5.80
006	Pacoima microcline	Ks_{88}	10.36	79.12	10.52	Ks_{7}	90.14	6.23	3.63
007	MJ39 interm. microcline	Ks_{88}	10.72	80.79	8.49	Ks_{8}	85.06	7.35	7.59
008	Zion amazonite	Ks_{92}	7.76	86.46	5.79	Ks_{4}	94.96	4.30	0.74
009L	LGDP orthoclase light	Ks_{85}	14.70	80.43	4.87	Ks_{11}	78.22	9.86	11.92
009H	LGDP orthoclase heavy	Ks_{81}	18.94	78.55	2.51	Ks_{5}	69.04	3.28	27.68
010	sanidine	Ks_{87}	12.19	84.65	3.15	Ks_{6}	92.96	6.15	0.90
011	Na-plagioclase	An_{31}	68.22	1.06	30.72	Ks_{78}	18.35	66.62	15.03
012	Brazil amazonite	Ks_{91}	8.09	85.76	6.15	Ks_{8}	91.61	7.47	0.92
013	Ethiopia amazonite	Ks_{95}	4.76	89.01	6.23	Ks_{7}	91.94	7.20	0.86
014	Russia amazonite	Ks_{92}	8.04	86.86	5.11	Ks_{7}	91.71	7.22	1.07

Table 2

Sample	Name	Composition	Monoclinic t_1	Triclinic $t_1o + t_1m$	Triclinic $t_1o - t_1m$	Triclinic t_1o
001	MJ40 labradorite	An_{67}				
002	San Gabriel labradorite	An_{68}				
003	Haystack amazonite	Ks_{94}		1.07	0.98	1.02
004	Papoose microcline	Ks_{84}		0.92	1.02	0.97
005	LGDH microcline	Ks_{90}		1.02	1.13	1.07
006	Pacoima microcline	Ks_{88}		0.99	1.04	1.01
007	MJ39 intermediate microcline	Ks_{88}		0.86	0.41	0.64
008	Zion amazonite	Ks_{92}		0.91	1.01	0.96
009L	LGDP orthoclase light	Ks_{85}	0.42			
009H	LGDP orthoclase heavy	Ks_{81}	0.42			
010	sanidine	Ks_{87}	0.40			
011	Na-plagioclase	An_{31}				
012	Brazil amazonite	Ks_{91}		* 0.29	* 1.93	* 1.11
013	Ethiopia amazonite	Ks_{95}		0.80	0.97	0.88
014	Russia amazonite	Ks_{92}		1.01	1.01	1.01

*likely measurement error

Table 3

3.1. K-Feldspars

3.1.1. Main K-feldspar group

Samples in this group include all of the K-feldspars except the amazonites and sample 010 sanidine.

3.1.1.1. 004 Papoose microcline

Sample 004, also known as Papoose microcline, was collected on 5 July 2013 from the core of the Papoose Flat pluton in the Inyo Mountains, about 30 miles southeast of Big Pine, CA. Coordinates are within a few hundred feet of N 37.022 W 118.119. The sample consists of K-feldspar megacrysts extracted from Papoose Flat quartz monzonite; unit **Kpf** on the USGS geologic map of the Waucoba Mountain quadrangle (Nelson, 1966). It is described as "light-colored, coarse-grained, porphyritic quartz monzonite, strongly foliated in border zone". The collected sample is from the core of the pluton and exhibits only light foliation. Sylvester et al. (1978) gives the age of the pluton as 75 – 81 my and describes it further as a coarse-grained biotite quartz monzonite with K-feldspar megacrysts up to 2 cm. The host rock of 004 Papoose microcline appears to have more muscovite than biotite but otherwise matches this description. Its K-feldspar megacrysts are 0.5 to 2 cm long and white. While some of them appear to be intergrown with other minerals, these sections were avoided after sledging when choosing pieces for crushing. The average composition of the non-lamellar areas was found to be Ks_{84}, while that of the lamellae was Ks_{7}. SEM analysis also revealed the occasional microscopic euhedral accessory zircon. XRD analysis matched 004 Papoose with an ordered microcline.

3.1.1.2. 005 LGDH microcline

Sample 005, also known as LGDH microcline, was collected 25 May 2013 from a roadcut on the Angeles Forest Highway, coordinates N 34.368683 W 118.103600 in the San Gabriel Mountains, Los Angeles County, CA. On the Dibblee Geological Foundation (DGS) geologic map of the Chilao Flat quadrangle (Dibblee & Minch, 2002), this location is part of the Lowe Granodiorite: "(of Miller, 1934) gray white, medium grained granitic rocks, granodiorite to quartz monzonite; moderately coherent, composed mostly of sodic plagioclase feldspar, potassic feldspar (orthoclase), as grains and large phenocrysts, quartz, hornblende, and biotite mica; age early Triassic (220± my, Ehlig, 1981); divided into zones by Ehlig, 1981". The map unit **LGDH** is described as "hornblende granodiorite lowest SW zone; light gray, richly mottled with black clusters of hornblende; contains minor orthoclase phenocrysts". The overall color of the host rock for sample 005 LGDH is light pinkish grey. The specimen is lightly to moderately foliated with some bands of green-black hornblende, but garnet is much more in abundance here, mostly as very small crystals but with some phenocrysts as large as 0.5 cm. Phenocrysts of what appear to be very dark blue-grey labradorite crystals also occur up to 1 cm long. The salmon pink K-feldspars dominate the texture and occur both as bands around 2 cm thick and phenocrysts over 4 cm long. Once sledged, pieces visually free of intergrowths were easy to select for crushing. The average composition of the non-lamellar areas was found to be Ks_{90}, while that of the lamellae was Ks_7. SEM analysis also revealed the presence of barium in some grains. The accelerating voltages of the SEM used for these measurements are not optimal for detecting Ba. However, the peaks were manually checked and confirmed to be barium. The reported composition of up to 0.3% BaO by mole is probably an underestimate. XRD analysis matched sample 005 LGDH with an ordered microcline, not the orthoclase as stated by Ehlig (1981). However, its luminescence behavior in some of the experiments may be

somewhat anomalous when compared to the other K-feldspars and particularly microclines; see Sections 5 and 6 for further discussion.

3.1.1.3. 006 Pacoima microcline

Sample 006, also known as Pacoima microcline, was collected on 2 November 2013 from a location in Pacoima Canyon, in the San Gabriel Mountains, Los Angeles County, CA. A large angular cobble about 20 cm in diameter was collected from the talus at the base of a steep ravine containing an allanite pegmatite pod at the top, somewhere near coordinates N 34.376 W 118.270. The pegmatite is within the unit **jgb,** described as a "Jotunite-norite-gabbro-diorite mafic complex" in the anorthosite-gabbro complex by the DGS geologic map of parts of the Sunland and Burbank quadrangles (Dibblee & Ehrenspeck, 1991). The pegmatite is described further by Neuerberg (1954) and Carter (1982). The cobble is mostly massive quartz, but one end has a 3 cm "cap" of dirty salmon pink K-feldspar. The two minerals appear to be separated by a discrete border, and do not seem to be intergrown on a visual scale. Exsolution lamellae are abundant and visible to the naked eye in the K-feldspar, with some stringers being up to 1 mm thick. The average composition of the non-lamellar areas was found to be Ks_{88}, while that of the lamellae was Ks_{7}. This sample was originally assumed to be a microcline due to its pegmatitic origins, and XRD analysis confirmed sample 006 Pacoima as a maximum microcline.

3.1.1.4. 007 MJ39 intermediate microcline

Sample 007, also known as MJ39 intermediate microcline, is a sample owned by UCLA's Luminescence Lab and prepared by W. E. Reed several years ago. Nothing further is known of its provenance. It is a large jar of K-feldspar (Ks_{88}; lamellae Ks_{8}) grains of particle size 1-2 ϕ (250-500 μm). The grains are a light

salmon pink in color. Sample 007 MJ39 was not crushed and sieved to 175-200 µm but was used at original grain size. XRD analysis matched sample 007 MJ39 with an intermediate microcline.

3.1.1.5. 009 LGDP orthoclase

Sample 009, also known as LGDP orthoclase, was collected 25 May 2013 from a roadcut on the Angeles Forest Highway, coordinates N 34.384750 W 118.099450 in the San Gabriel Mountains, Los Angeles County, CA. On the DGS geologic map of parts of the Pacifico mountain and Palmdale quadrangles (Dibblee & Ehrenspeck, 2001) this location is part of the Lowe Granodiorite: "plutonic igneous rocks with variable but average composition of granodiorite; light gray to tan; hard but much fractured, massive to slightly gneissoid; composed of mostly sodic plagioclase feldspar, lesser quartz and potassic feldspar, minor biotite as minute flakes; probably early Triassic age, 220± m.y. old (Silver, 1968; 1971; Ehlig, 1981)". The map unit **LGDP** is further described as "gray, contains large phenocrysts of potassic feldspar and clustered hornblende, locally contains euhedral garnet crystals or clusters up to 1 cm in size; partly gneissoid". The visually striking host rock of the collected sample 009 well matches this description. The author has found euhedral garnet crystals as large as 2 cm, and the pinkish-grey lavender K-feldspar megacrysts are as large as 12 cm long and 5 cm wide. It is hard but very fractured, making sledging an easy task. Some of the very large K-feldspar crystals had intergrowths of the groundmass (assumed to be microscopic plagioclase and quartz crystals). Enough material was collected so that these sections could be avoided when selecting pieces for further crushing. XRD analysis matched sample 009 LGDP with an orthoclase.

3.1.1.5.1. 009L LGDP light and 009H LGDP heavy

Unlike any of the other samples, the 175-200 µm sieved grains of 009 LGDP was separated into two portions: those less than a specific gravity of 2.565, and those greater using a "super-K", or "SuK" method. This procedure is described in Section 4.1 These two samples are called 009L ("light") and 009H ("heavy"). The non-lamellar areas of 009L grains were found to have an average of Ks_{85} and the lamellae a composition of Ks_7 (the most potassic of any of the K-feldspar samples' lamellae), while 009H was Ks_{81} (unsurprisingly the least potassic of all the K-feldspar samples) with lamellae composition of Ks_5. Like 005 LGDH microcline, the other sample from the Lowe Granodiorite, sample 009 showed distinctive barium peaks. The occurrence did not differ significantly between 009L and 009H (with an average of 0.48 and 0.46 mol% BaO respectively). Ba was only found in the K-rich portion of grains, not the Na-rich lamellae. Occasional microscopic euhedral titanite inclusions were observed in both portions.

3.1.2. Amazonite group

Several amazonite samples from at least four continents were included in this study because preliminary results on sample 003 Haystack pointed to fundamental differences between it and other samples with similar ordering and K-content. The XRD analysis matched all of these amazonite samples to maximum microclines. While the XRD analysis of 012 Brazil was thrown out due to clearly incorrect values (see Section 3.1.2.3 for further discussion), it too is likely a maximum microcline.

3.1.2.1. 003 Haystack

Sample 003, also known as Haystack amazonite, was collected on 7 July 2013 from a location ~4 miles east of Lone Pine, CA known locally as the Haystack and on geologic maps as Kern Knob. A small boulder about 30 cm in diameter was collected from a talus slope on the north side of the hill, coordinates N 36.621322 W 117.993375. It is found on the unit named **Kk**, Kern Knob Granite, by the USGS geologic map of the Lone Pine quadrangle. Its description says it "contains locally abundant… pegmatite lenses and dikes that consist primarily of microcline and quartz, with less abundant amazonite. Biotite $^{40}Ar/^{39}Ar$ plateau age 91 Ma" (Stone et al., 2000). A much more detailed description can be found in Griffiths (1987). The host rock for 003 Haystack consisted of microcline, of both the common white variety and dilute to bright light green amazonite, light grey to smoky quartz, and occasional black biotite. Amazonite crystals were as long as 3 cm, but much more commonly were around 0.5 cm. Individual crystals were coherent and had little fracturing, but the rock was easily separated along grain boundaries given a moderate tap with a sledgehammer. Green amazonite pieces were hand selected and given two 10-min baths in 3% hydrochloric acid to remove a calcite crust observed during sample preparation. These pieces were then crushed and sieved in the same manner as the other samples. The average composition of the non-lamellar areas was found to be Ks_{94}, while that of the lamellae was Ks_9. SEM analysis also revealed inclusions of microscopic, euhedral zircon crystals, as well as small isolated patches of concentrated thorium (see Figure 4). XRD analysis confirmed 003 as a maximum microcline.

Figure 4 SEM BSE image of 003 Haystack amazonite. Brighter areas indicate higher average atomic number Z. Note the euhedral accessory zircon in the top left of the image; the bright patch in the lower right is concentrated thorium.

3.1.2.2. 008 Zion

Sample 008, also known as Zion amazonite, was purchased from Zion Rock and Gem in Springdale, Utah on 14 August 2013. Nothing further is known of its provenance. It is a darker pastel green with hints of blue. The original sample before processing had dimensions of about 3 cm on a side. Part of the sample appeared to be intergrown with quartz, and other sections grade back to pink microcline; these areas were avoided when choosing pieces for crushing. White lineations less than a millimeter observed running through the sample were assumed to dissolution features of some kind. The average composition of the non-lamellar areas was found to be Ks_{92}, while that of the lamellae was Ks_4, the least potassic of any of the K-feldspar samples' lamellae. XRD analysis confirmed 008 as a maximum microcline.

3.1.2.3. 012 Brazil

Sample 012, also known as Brazil amazonite, came from a 1-pound bag of elongated tumbled stones 2-4 cm in length. It was purchased from Jewel Tunnel Imports in Baldwin Park, CA on 22 November 2014. Other than being from Brazil, nothing further is known of its provenance. It is a brighter blue-green than 008 Zion. A single stone was used from this bag in case the stones came from multiple localities. Since this tumbled and polished sample had been obviously processed in some way, all outer surface area was removed with a small jewelry saw in case it had been chemically altered (such as being impregnated with wax to deepen the color). The resulting section was about 1-2 cm on a side before crushing. The average composition of the non-lamellar areas was found to be Ks_{91}, while that of the lamellae was Ks_{8}. XRD analysis matched 012 with an ordered microcline. However, calculations of Al,Si order using cell parameters refined from this match gave impossible results: ($t_1o - t_1m$) was computed to be 1.93, while the maximum possible value is 1 (see Sections 2.1.2 and 4.3 for further information). The unit cell parameters also varied noticeably from the other amazonites (see the XRD calculated cell parameters spreadsheet in supplementary materials). This match was likely in error and thus sample 012 Brazil was not included in analyses comparing Al,Si order with luminescence characteristics, although the sample is still likely to be a maximum microcline, like the other four amazonites.

3.1.2.4. 013 Ethiopia

Sample 013, also known as Ethiopia amazonite, was originally a single crystal hand specimen about 4 cm in length. It was purchased from Jewel Tunnel Imports in Baldwin Park, CA on 22 November 2014. Its sample tag lists it as being from “Konso, Southern Nations and Nationalities, Regional State, Ethiopia”. It is a brighter blue-green than 008 Zion. In case the sample had been chemically altered in some way (such as soaking in oxalic acid to remove limonite staining), all outer surface area was cut off with a

small jewelry saw. The color is a light pale blue-green, similar to 008 Zion but more washed out. The average composition of the non-lamellar areas was found to be Ks_{95}, the highest of all the samples, while that of the lamellae was Ks_{7}. XRD analysis confirmed 013 Ethiopia as a maximum microcline.

3.1.2.5. 014 Russia

Sample 014, also known as Russia amazonite, came from a single tumbled stone 1-2 cm in length. It was purchased from a booth owned by IKON Mining & Exploration (headquarters in Fallbrook, CA) in the Exhibition Hall at the AGU Fall Meeting, 15 – 19 December 2014. Other than being from Russia, nothing further is known of its provenance. It is a deep striking green the color of malachite. Visible exsolution lamellae thicker than 1 mm cover the surface and are a tannish white. Since this tumbled and polished sample had been obviously processed in some way, all outer surface area was removed with a small jewelry saw in case it had been chemically altered (such as being impregnated with wax to deepen the color), although the interior turned out to be just as green as the exterior. The average composition of the non-lamellar areas was found to be Ks_{92}, while that of the lamellae was Ks_{7}. XRD analysis confirmed 014 Russia as a maximum microcline.

3.1.3. 010 Sanidine

Sample 010, also known as UCLA sanidine, is a specimen owned by UCLA's Earth, Planetary, and Space Sciences (EPSS) Department and used in many introductory geology courses. Nothing further is known of its provenance. The author was kindly allowed to remove a small slice with a rock saw for use in this research. The original hand sample is glassy, translucent, and white. The average composition of the non-lamellar areas is Ks_{87} and that of its lamellae is Ks_{6}. Phosphorus was also found, with an average of

0.22 mol% P_2O_5 in the potassic sections, but only 0.05 mol% in the sodic sections. XRD analysis matched 010 with a sanidine.

3.2. Plagioclases

3.2.1. Labradorites (calcic plagioclases)

3.2.1.1. 002 San Gabriel labradorite

Sample 002, also known as San Gabriel labradorite (or sometimes anorthosite), was collected 25 May 2013 from a roadcut on the Angeles Forest Highway near mile marker 13.89, coordinates N 34.360933 W 118.108967 in the San Gabriel Mountains, Los Angeles County, CA. On the DGS geologic map of the Chilao Flat quadrangle (Dibblee & Minch, 2002) this location is part of the Anorthosite Gabbro Complex: "unusual plutonic complex of plagioclase feldspar rich rocks and associated dark mafic rocks of Western San Gabriel Mtns; medium grained, massive; coherent, but much fractured; age Precambrian (Carter, 1980, 1982; Ehlig, 1981)". The map unit **an** is described as "anorthosite, light steel gray, but weathered white; composed almost entirely of sodic plagioclase (andesine [An_{30-50}]) feldspar". The exterior weathered sections of 002 are white and powdery, and appear to have altered to muscovite and possibly some light-green chlorite. These areas were avoided when choosing sections for crushing. The interior ranges in color from light grey to a dark blue-grey, with very small inclusions of dark green hornblende. Cleavage planes of the dark bluish sections sometimes display faint labradorescence. Unlike the description in Dibblee and Minch (2002), the composition of crushed feldspar grains in 002 was found to range from An_{65} to An_{75}, with the average being An_{68}, or labradorite (see Figure 1). This locally well-known rock unit is often described as "labradorite" (or the more colloquial "moonstone") by

rockhounds, mineral collectors, and lapidary enthusiasts. The closest match during XRD analysis was also a labradorite.

3.2.1.2. 001 MJ40 labradorite

Sample 001, also known as MJ40 labradorite, is a sample owned by UCLA's Luminescence Lab and prepared by W. E. Reed several years ago. It is it is a large jar of calcic labradorite plagioclase (An_{67}) grains of particle size 1-2 ϕ (250-500 μm). The grains range in color from white-grey to very dark grey, with overall average being a light grey. Sample 001 MJ40 was not crushed and sieved to 175-200 μm but was used in its original grain size. Given that the SEM compositions, XRD cell parameters, and IRSL behaviors are all very similar to sample 002 (described in Section 3.2.1.1), it is probable that 001 MJ40 was also collected from the San Gabriel anorthosite, a well-known local source of plagioclase of this composition.

3.2.2. 011 Andesine (sodic plagioclase)

Sample 011, also known as UCLA andesine or Na-plagioclase, is a sample owned by UCLA's EPSS Department and used in many introductory geology courses. Nothing further is known of its provenance. The author was kindly allowed to remove a small slice with a rock saw for use in this research. The original hand sample is white and slightly translucent. Although the sample is labeled "albite", the average non-lamellar composition is An_{31}, making 011 an andesine (An_{30-50}). Some grains contained K-rich areas; while most of the sample contains relatively little potassium, these sections have an average composition of Ks_{78}. XRD analysis matches 011 with an ordered calcian albite. This database match may be following the International Mineralogical Association (IMA) convention of nomenclature, where a solid-solution series is arbitrarily divided at 50 mol% into two portions named after their

endmembers (Nickel, 1992). In this naming system An_{31} would be considered a calcian albite; therefore the SEM and XRD analyses for this sample are likely in agreement.

Sample 011 is generally referred to as “011 Na-plagioclase” instead of the more precise “011 andesine” so as not to confuse it with the very-similar-sounding sample 010 sanidine, as well as to emphasize the fundamental differences in behavior between this sample and the more calcic labradorite samples.

4. Methods

4.1. Sample Preparation

Fifteen samples were analyzed for this research, and are described in detail in Section 3. Table 1 summarizes their physical properties and other details. Since all the samples been exposed to daylight and this research was not targeting the naturally-induced signal, preparation was done under normal lighting conditions instead of in a darkroom. Etching with hydrofluoric acid is part of the routine sample preparation for pIRIR dating in some laboratories and is used to remove the alpha-irradiated rims of the sediment-extracted grains, which improves their transparency for stimulation light and IRSL emissions (Rhodes, 2015). As the feldspars in this research were crushed directly from their parent crystals and spent no time weathering in the environment, this procedure was not applied to any of the samples.

When possible, representative unprocessed example specimens were retained for each numbered sample. 003 Haystack amazonite, 004 Papoose microcline, 005 LGDH microcline, and 009 LDGP orthoclase were collected within their host rock. Sledgehammers, rock hammers, and chisels were used to separate the feldspar crystals from the matrix.

003 Haystack amazonite had coherent crystals around 0.5 cm in length that easily separated along grain boundaries without being crushed if hammered carefully. These showed evidence of an interstitial weathered calcite crust. Green amazonite pieces were hand selected and given two 10-min baths in 3% hydrochloric acid to remove the crust. No other chemical alterations were performed on the samples.

The purchased amazonites 012 Brazil, 013 Ethiopia, and 014 Russia all had their outer surface area carefully trimmed off with a small jewelry saw to remove any material affected by possible lapidary

treatment with wax (to deepen color) or oxalic acid (to remove iron oxide staining). This procedure was not conducted on 008 Zion amazonite, purchased and processed earlier in the research. However, as this sample was significantly cheaper in price, it is less likely to have received such "aesthetic enhancement" treatment prior to sale.

All of the samples were then broken into pebble-sized fragments by sledgehammer if not already small enough. The pieces were visually inspected, and those that appeared to be uniformly feldspar were selected for crushing with a Plattner-style three-piece hardened steel mortar and pestle with the assistance of a hammer.

The crushed samples were dry-sieved and the larger grains re-crushed until there was enough material in the 175-200 µm portion for both SEM and IRSL analyses. The XRD tests applied work best with grain sizes of around 10 µm (Pecharsky & Zavalij, 2009). As the smallest sieve screen easily available was 100 µm, the <100 µm portion was ground by hand with a ceramic mortar and pestle until powdered.

The Super-K (SuK) method, as introduced by Rhodes (2015), is a centrifuge floatation separation technique that uses the heavy liquid lithium metatungstate (LMT) with a specific gravity of 2.565, instead of the more typically used 2.58. Alkali feldspars whose bulk compositions are more highly potassic are generally found to have greater sensitivity (see Section 2.2.1). Since K-feldspars are less dense than Na-feldspars, this method attempts to select grains more favorable for IRSL dating. Preliminary results indicated that in one case of grains extracted from a New Zealand sediment using the SuK method, the net IRSL sensitivity increased by a factor of almost 100 compared to the conventional separation procedure.

The SuK method was used on the 175-200 µm portion of sample 009 LGDP orthoclase, yielding two samples. 009L LGDP light refers to grains with a specific gravity less than 2.565, and 009H LGDP heavy

are the grains heavier than 2.565. The portion of 009 LGDP analyzed using XRD was not separated. None of the other samples were subjected to heavy liquid separation.

The museum samples 001 MJ40 labradorite and 007 MJ39 intermediate microcline were already crushed to grain sizes of 250-500 μm, and were not further reduced for IRSL and SEM analyses. Metal shavings (confirmed as iron-bearing by SEM analysis) were observed in both of the samples, possibly a byproduct of the original crushing process. These shavings were large enough to avoid during IRSL disc mounting, and did not interfere with SEM analysis of the feldspar grains. As much of this contamination as possible was removed prior to powdering a portion for XRD analysis by repeatedly dragging a hand magnet through the samples.

4.2. Scanning Electron Microscope

A scanning electron microscope (SEM) was used to analyze samples for composition and lamellae content. A TESCAN VEGA3 SEM owned by the UCLA EPSS department was used for all SEM analysis. Several hundreds of grains per sample, prepared as described in the section above, were adhered to a standard SEM aluminum pin stub mount using PELCO-brand double-coated, conductive carbon adhesive tabs. As the grains were uncoated, all measurements were taken in low vacuum mode at a pressure of 5 Pa instead of high vacuum to minimize surface charge buildup due to the use of an accelerating voltage of 30 KeV. A scintillation-type backscattered electron (BSE) detector was used to take images. These scans illustrate compositional contrasts: areas with a lower average atomic number Z appear darker, while brighter sections have higher average Z (see Figure 4). BSE images are good for rapid phase discrimination such as identifying exsolution lamellae (Egerton, 2005).

Areas with a representative variety of grains and lamellae morphologies were selected. A composition map using an EDAX-brand energy dispersive spectroscopy (EDS) instrument was taken at 170x magnification to identify which sections of selected grains to analyze further. Then, a representative variety of 7-9 grains were selected and 3 EDS measurements taken of each grain. If grains had lamellae or other Na-rich areas (or K-rich areas, for the plagioclases), up to 3 measurements were taken per grain of those as well. They were analyzed for elements Na, Al, Si, K, Ca, Fe, and O, though results were recorded as mol% oxide for convenience. The background noise was determined automatically by EDAX's proprietary TEAM™ software but manually tweaked before it was subtracted from the EDS spectrum when calculating composition. When there were obvious peaks from other elements besides C (presumably from the carbon tape), these were noted (see Table 1).

Spot compositions were individually checked, and some were thrown out due to very low counts, ambiguous results, or grains that turned out not to be the target feldspar. The rest of the spots were plotted on a ternary diagram with the help of a spreadsheet by Graham and Midgley (2000) and averaged to get the mean non-lamellar composition of each sample (Figure 5). Note that this is a different measurement from the bulk composition, as it does not include the compositional contribution of the lamellae. For example, a hypothetical perfectly-exsolved alkali feldspar would have completely partitioned all of its Na into exsolution lamellae, leaving the non-lamellar areas with a composition of Ks_{100} and a lamellae composition of Ks_0 (Ab_{100}). If 10% of the crystal was composed of these lamellae, its bulk composition would thus be Ks_{90}.

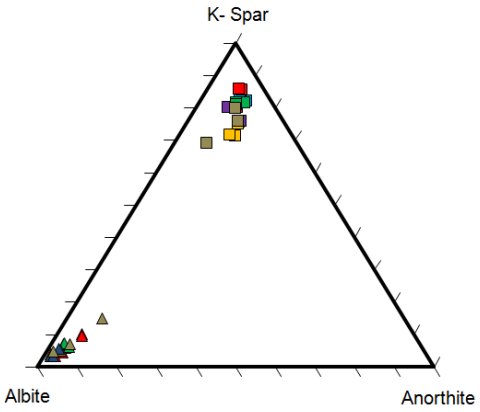

Figure 5 SEM composition measurement of sample 006 Pacoima microcline. Squares are spot measurements in non-lamellar areas; triangles are lamellae spots. Shapes of the same color are measurements of the same grain.

One limitation of this method the author observed was overestimation of Ca content in K-feldspars. The peaks for K and Ca are very close together, so the TEAM™ software may report some Ca in a sample with high K content even if no calcium is present (Egerton, 2005). The amount is never high, but it sometimes can push a K-feldspar sample into the "forbidden zone" of more than An_{5-10}. Since there was no planned analysis of Ca content of the K-feldspars, and it does not affect the Ab-Ks ratio, it was decided to report composition of K-feldspars based on Ab-Ks ratio alone. The same was done with the Ab-An ratio (ignoring the Ks portion) for the three plagioclases.

4.3. X-Ray Diffraction

X-ray diffraction (XRD) analysis was used to measure cell parameters for the samples, which were used to calculate Al,Si ordering in the K-feldspar samples. It was also used to broadly confirm composition of the samples from SEM analysis. A PANalytical X'Pert Pro X-ray Powder Diffractometer owned by the UCLA Molecular Instrumentation Center was used for all XRD analysis. Samples were mounted on a spinning stage and continuously scanned from 2θ = 5-70° at a rate of 0.05 $2\theta^{\circ}$/sec. A few samples did not have enough material to be measured on the spinning stage, and were measured in a smaller stationary bracket. These were samples 005 LGDH microcline, 006 Pacoima microcline, 010 sanidine, and 014 Russia amazonite.

PANalytical proprietary software X'Pert HighScore Plus was used to manually fit and subtract the background noise before automatically identifying peaks in the XRD pattern. These peaks were manually confirmed, then the International Centre for Diffraction Data's Powder Diffraction database was searched for reference patterns matching these peak positions, and the candidate with the highest match score (as determined by the proprietary software) was selected. The software used this reference

pattern to assign Miller indices to the peaks in the measured data, giving approximate values of the cell parameters: vectors *a*, *b*, and *c*, and angles α, β, and γ (Pecharsky & Zavalij, 2009). A least-squares calculation was used by the HighScore program to further refine the unit cell parameters.

T_1 and T_1o aluminum occupancy was calculated using three equations given by Kroll and Ribbe (1983), which take advantage of the change in unit cell size and shape due to the difference in oxygen bond lengths of Al and Si. For the monoclinic K-feldspars:

$$2\mathrm{t}_1 = -7.590 - 2.325b + 5.3581c$$

Equation 8

For the triclinic K-feldspars:

$$\mathrm{t}_{1\mathrm{o}} + \mathrm{t}_{1\mathrm{m}} = \frac{b - 0.7138 - 1.7505c}{-7.7245 + 1.0150c}$$

Equation 9

and

$$\mathrm{t}_{1\mathrm{o}} - \mathrm{t}_{1\mathrm{m}} = \frac{\alpha^* + 89.118 - 1.9902\gamma^*}{-24.691 + 0.229\gamma^*}$$

Equation 10

where α^* and γ^* are reciprocal cell parameters calculated from the direct cell parameters (Rupp, 2013). Equation 8 can be divided by 2 to give t_1 for monoclinic K-feldspars, and Equation 9 and Equation 10 can be added to give t_1o for the triclinic ones (Kroll & Ribbe, 1983; Pecharsky & Zavalij, 2009).

Some of the results calculated in this research for t_1o or t_1m fell slightly outside of physically possible values. As the absolute numbers are not important to this study, just the relative difference in ordering

between the samples, it is assumed these errors are systematic and they have not been altered (Table 3 and the XRD calculated cell parameters spreadsheet in supplementary materials). However, sample 012 Brazil amazonite gave a clearly impossible result, likely due to erroneous matching to an incompatible XRD reference pattern, and this sample was not used in Al,Si ordering analysis.

4.4. Infrared Stimulated Luminescence

Multiple-grain aliquots were prepared by adhering a single layer of sample grains to a 9.7 mm diameter aluminum disk using high viscosity silicon oil. These disks were then sprayed with a clear acrylic to help protect them for later archiving. A few samples analyzed early on did not receive this treatment: samples 001 MJ40 labradorite, 007 MJ39 intermediate microcline, 009L LGDP orthoclase light, 003 Haystack amazonite, and 008 Zion amazonite. Based on measurements of sprayed discs with no grains, the acrylic is not believed to have any effect on the IRSL measurements (Rhodes, 2016, personal communication).

These discs were put into a Risø TL-DA-20 TL-OSL reader. A slightly modified version of the dating protocol developed by Buylaert et al. (2009) and summarized in Table 4 was used as the basis for these measurements, which also forms the basis of single grain post-IR IRSL dating measurements (e.g. Brown & Rhodes, 2015; Rhodes, 2015). At the start of each session, the sample was given a “hot bleach” by stimulation with IR diodes for 40 seconds at a temperature of 290°C. This is intended to “reset” the sample by liberating any remaining trapped charge from natural signals or previous analysis runs. A standard dating measurement cycle, or “run”, is as follows: the sample is given a standard dose of 100 seconds of beta radiation (approximately 10 gray). It is then preheated for 60 seconds at 250°C. The first IRSL measurement (often referred to as IR_{50}) is taken at 50°C for 100 seconds. The second, or “post-IR IRSL” (pIRIR, or sometimes IR_{225}) measurement is taken at 225°C, also for 100 seconds. It is this

measurement that is used for most analysis in this research. Next a test dose of 30 seconds of beta radiation (approximately 3 Gy) is given, followed by standard IR_{50} and IR_{225} measurements at 100 seconds each. The results of these can be checked if the luminescence properties of the sample is suspected to be changing between runs. Finally the sample is given another hot bleach to "reset" the sample for the next measurement cycle.

		Standard Protocol		***Experimental Protocols***		
Step		**Time**	**Temp**	***Time***	***Temp***	***Exp #***
1	Beta dose	100 s (~10 Gy)				
2	Preheat (TL)	60 s	250°C		*150-300°C*	*1*
3	First IR (IRSL)	100 s	50°C	*0.25-300 s*	*50-225°C*	*(time) 3* *(temp) 4*
--> 4	**pIRIR (IRSL)**	100 s	225°C		*100-225°C*	*2*
5	Test beta dose	30 s (~3 Gy)				
6	Test Preheat (TL)	60 s	250°C			
7	Test IRSL	100 s	50°C			
8	Test IRSL	100 s	225°C			
9	Hot bleach (IRSL)	40 s	290°C			

Table 4

There were four experiments conducted, observing the changes in IRSL properties when measurement parameters were varied. In other words, the IRSL measurements were designed to explore variations in response between samples for each treatment, and to explore how modified treatments might perform. Each experiment consisted of six to eight runs of each disc. The first experiment varied the preheat temperature (normally 250°C) from 150-300°C in steps of 25°, but maintained the preheat time of 60 seconds. The second experiment varied the pIRIR measurement temperature (normally 225°C) from 100-225°C in steps of 25°. The third experiment varied the measurement time of the first IR measurement (normally 100 s) from 0.25 to 300 seconds in roughly half order of magnitude steps (0.25,

1, 3, 10, 30, 100, and 300 seconds). The fourth experiment varied the measurement temperature of the first IR measurement (normally 50°C) from 50-225°C degrees C in steps of 25° but kept the duration as 100 seconds. While some of these protocol combinations access parts of the signal thought to be thermally unstable or otherwise unsuitable for dating (such as having a preheat temperature below the pIRIR measurement temperature), this study is more concerned with how these charge populations may vary in different feldspars (Buylaert et al., 2009).

The experiments measured the IRSL counts in each of 250 channels. As all of the pIRIR measurements in this study were 100 seconds long, each channel corresponds to 0.4 seconds. The built-in MATLAB function "lsqcurvefit" (linear regression model, fitted using the least squares approach) was used to calculate the parameters I_0', a, p, and B_{abs} to give the decay equation

$$I = \frac{I_0' - B_{abs}}{(1 + at)^p} + B_{abs}$$

Equation 11

the best fit to the measured data (modified from Bailiff and Barnett (1994); see Section 1 for details). In this version of Equation 11, intensity I is the IRSL count at time t. Initial intensity I_0', sometimes called brightness, is defined as the maximum count of all the channels. Most of the decays in this study were well behaved, so this usually corresponded to the value in the first channel. Absolute background B_{abs} represents the sum of R (any signal components from the sample with slow enough decays such that they would appear constant on the order of the measurement time of 100 seconds), plus any background noise (dark count from the photomultiplier tube, breakthrough of the optical stimulation source, etc.).

The aim of this research is to qualitatively identify patterns in changes in the luminescence parameters across experiments and between samples, rather than calculate quantifiable values. As there is a trade-off between *a* and *p* in fitting the shape of the decay, it was ultimately decided to hold *p* = 2 in these calculations to simplify these comparisons. This value was chosen based on early calculations. The parameter *a* in this research is thus broadly interpreted as a measurement of how fast a signal decays, with a higher value indicating a faster decay. For convenience, Equation 11 was also normalized to I_0'. Thus the final form of the fitted equation is

$$\frac{I}{I_0'} = \frac{1 - B}{(1 + at)^2} + B$$

Equation 12

where $B = B_{abs}/I_0'$.

While fading corrections have not been applied, measurements were made soon after irradiation in all cases, so variations in anomalous signal fading, discussed in Section 2.2, are considered unlikely to be significant.

5. Results

Spreadsheets of calculated pIRIR decay parameters for each experiment may be found in the supplementary materials. Calculated parameters for the IR_{50} decay are also available for the first (preheat temperature) and third (IR_{50} time) experiments

A few remarks are necessary before systematically reviewing the highlights of the experimental results.

This thesis uses the term “coherent decay” to indicate that the signal can be reasonably well-fitted by Equation 12 while being high enough above the noise floor so that the calculated parameters can be trusted. An “incoherent decay” would result from very low brightness and/or lack of IRSL activity. The labradorites (samples 001 MJ40 and 002 San Gabriel) only have coherent decays for part of the first (preheat) and third (IR_{50} time) experiments.

Initial intensity I_0’ was generally assumed to be related to sensitivity; brighter samples show a greater response to applied dose, and are more ideal for dating. The meaning of parameter *a* is less clear, though higher values indicated a more quickly falling signal; such a sample would be assumed to bleach in sunlight faster, which is an important consideration for certain geological contexts where bleaching events may be very brief, such as a tsunami (Brill et al., 2012). However, there is a trade-off between bleachability (rate of signal reduction by light) and thermal stability, for both anomalous fading and regular fading, so any signal selected is a compromise. The parameter B was generally found to vary inversely with I_0’. This is to be expected: a constant value of added background noise would have a larger proportional effect on those samples with smaller IRSL intensities.

When looking at I_0’, a few general patterns are notable that hold for most of the experiments. All of the amazonites and sample 010 sanidine are dimmer than the main K-feldspar group. 009L LGDP orthoclase

light is brighter than its heavier counterpart 009H, but usually not by a significant amount. Sample 011 Na-plagioclase is comparable to the main K-feldspars in intensity at least, but the change in I_0' with the varied protocol parameter often has a subtly different shape. Finally, samples 006 Pacoima microcline and 007 MJ39 intermediate microcline are noticeably the brightest of all the samples; they generally have values of I_0' larger than others in the main K-feldspar group by factors of 2 or more.

The calculated parameters of the amazonite group tended to show a wide degree of variation between samples, and even different discs of the same sample. This may be due to the dimness of their decays in general, allowing background noise to have a proportionally larger effect on the precision of the calculated parameters, though it probably also has something to do with their amazonitic character (Pb content, perhaps). The amazonite group was often skipped when attempting to analyze patterns in the other K-feldspars between calculated decay parameters and Ks content or Al,Si ordering.

Decay parameters of the first IR measurement (IR_{50}, except for the fourth experiment) were generally not calculated for this research. However, a comparison was done of the I_0' of the $pIRIR_{225}$ signal with that of the first IR_{50} measurement for a standard dating protocol (see Table 4 for details). Figure 6 shows that the $I_0'_{225}/I_0'_{50}$ ratio for most of the samples was between 0.5 and 1.5. 011 Na-plagioclase's $pIRIR_{225}$ response is about an order of magnitude dimmer than that of IR_{50}. Both 009 LGDP orthoclase samples were noticeably higher than the main K-feldspar group, around 2. However, the most striking result belongs to 010 sanidine – Figure 7 shows that its $pIRIR_{225}$ response is about an order of magnitude brighter than for IR_{50}.

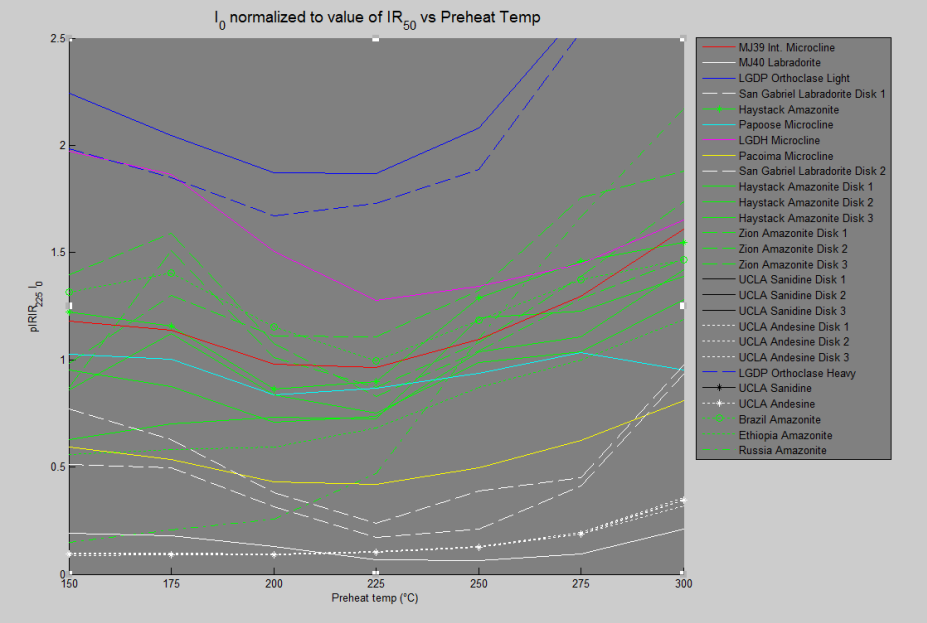

Figure 6 Ratio of initial brightness of $pIRIR_{225}$ and IR_{50} measurements ($I_0'_{225}/I_0'_{50}$) for Experiment 1, varying preheat temperature (PH).

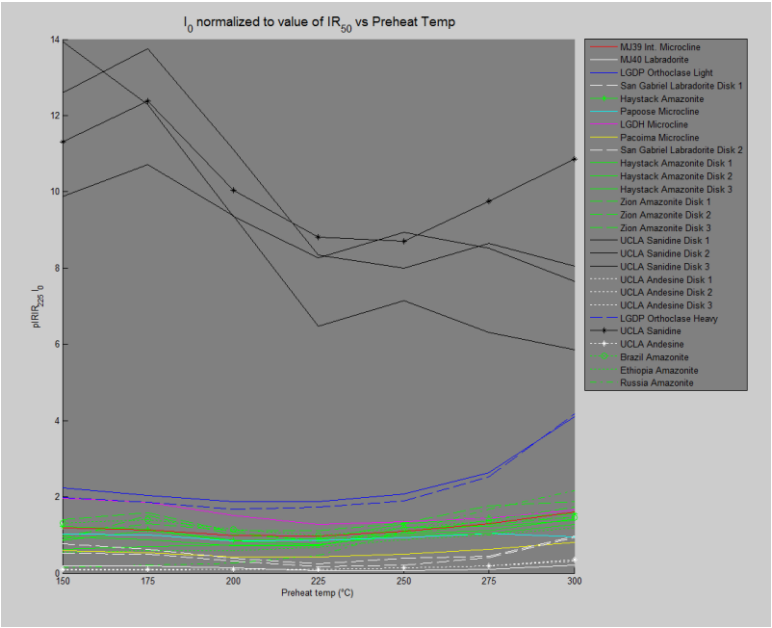

Figure 7 Ratio of initial brightness of $pIRIR_{225}$ and IR_{50} measurements ($I_0'_{225}/I_0'_{50}$) for Experiment 1, varying preheat temperature (PH). Same data as figure 6 but zoomed out to show 010 sanidine.

This $I_0'_{225}/I_0'_{50}$ ratio seems to correspond somehow with disorder (except for sample 005 LGDH) – 010 sanidine has the highest value, followed by 009 LGDP orthoclase heavy and light, then 007 MJ39 intermediate microcline, and finally the maximum microclines 004 Papoose and 006 Pacoima.

5.1. First Experiment: Preheat temperature

The first experiment varied the preheat temperature (PH) from 150-300°C in steps of 25°, maintaining the preheat time of 60 seconds. PH = 250°C in the standard dating protocol; see Table 4 for details.

The labradorites both exhibited weaker and weaker response with increasing preheat temperature. Above preheats of around 225°C (the same temperature as the $pIRIR_{225}$ measurement) the decay curves became incoherent, although I_0' continues to drop (Figure 8 and Figure 9). In contrast, sample 011 Na-plagioclase retained a well-defined decay curve throughout all tested preheat temperatures.

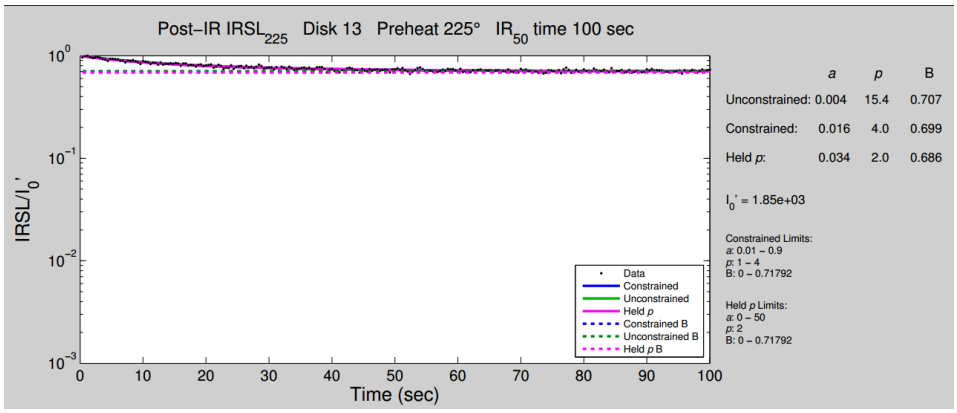

Figure 8 $pIRIR_{225}$ measurement of sample 002 San Gabriel labradorite at PH = 125°C. Only slight decay.

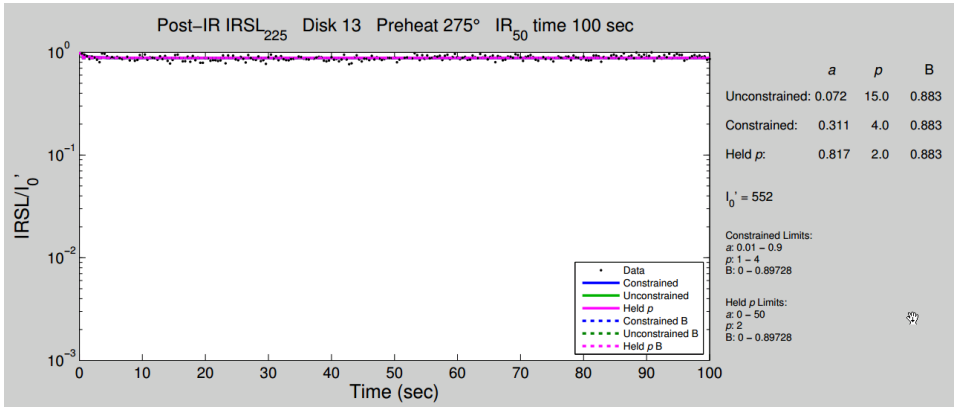

Figure 9 $pIRIR_{225}$ measurement of sample 002 San Gabriel labradorite at PH = 175°C. No coherent decay.

Initial IRSL intensity I'_0 decreases more or less monotonically with increasing preheat for all samples. It seems to decrease exponentially in the more well-behaved samples (the main K-feldspar group plus 011 Na-plagioclase) (Figure 10). Within the main K-feldspar group, the initial intensity seems to increase with increasing Ks content except for sample 005 LGDH microcline (Figure 11).

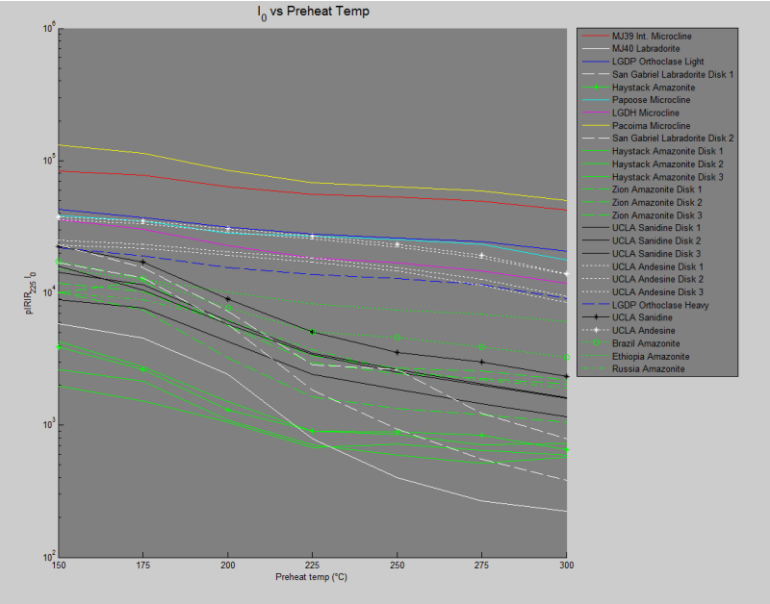

Figure 10 Experiment 1, varying preheat temperature (PH). PH vs. initial intensity I_0'. Note log axis.

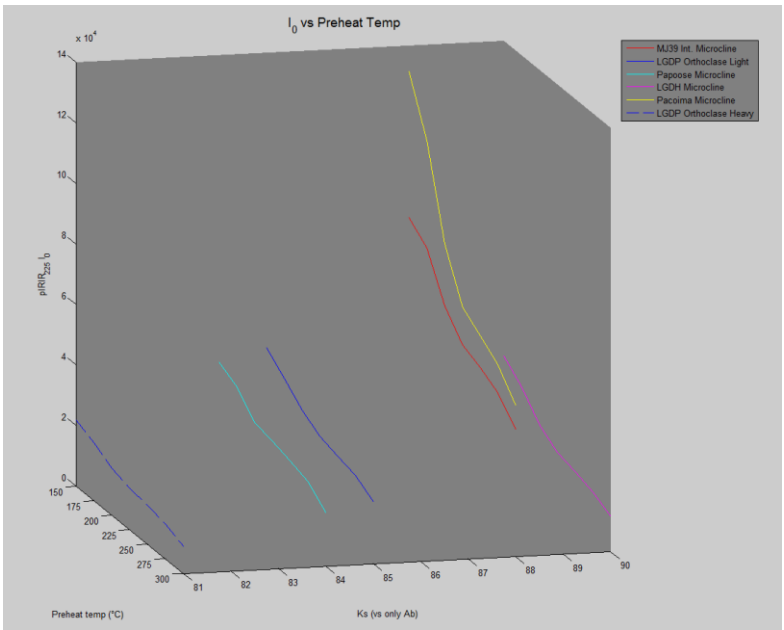

Figure 11 Experiment 1, varying preheat temperature (PH). PH vs. I_0'; each sample normalized to its I_0'value at PH = 250°C. Z-axis is Ks ($KAlSi_3O_8$) content in mol%.

When each sample's curve of preheat temperature vs. I'_0 is normalized to its value at 250°C, it becomes apparent that in the labradorites, and to a lesser extent sample 010 sanidine and the amazonites, I_0' drops proportionally faster with increasing preheat temperatures compared to the other samples.

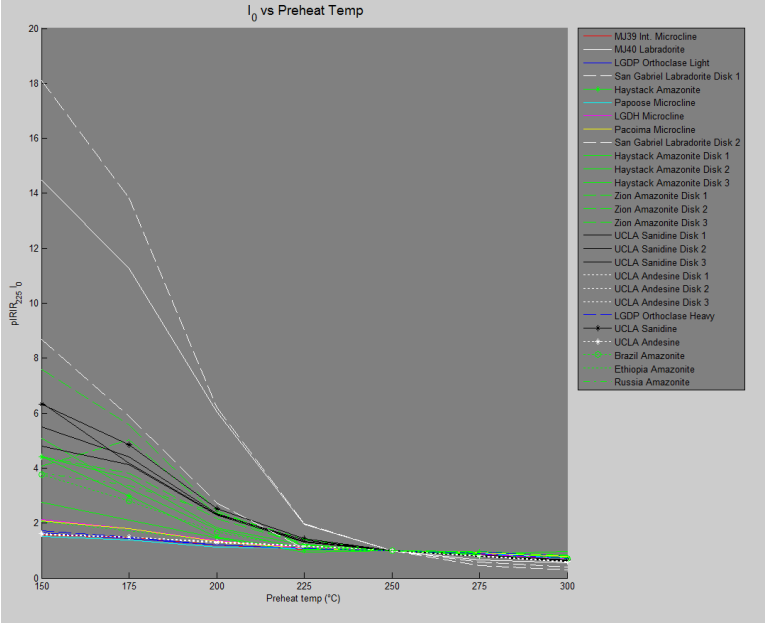

Figure 12 Experiment 1, varying preheat temperature (PH). PH vs. I_0'; each sample normalized to its I_0' value at PH = 250°C.

The initial intensity of 001 MJ40 labradorite is 14 times higher when measured with PH = 150°C compared to 250°C; I_0' of 006 Pacoima microcline only drops by a factor of 2.

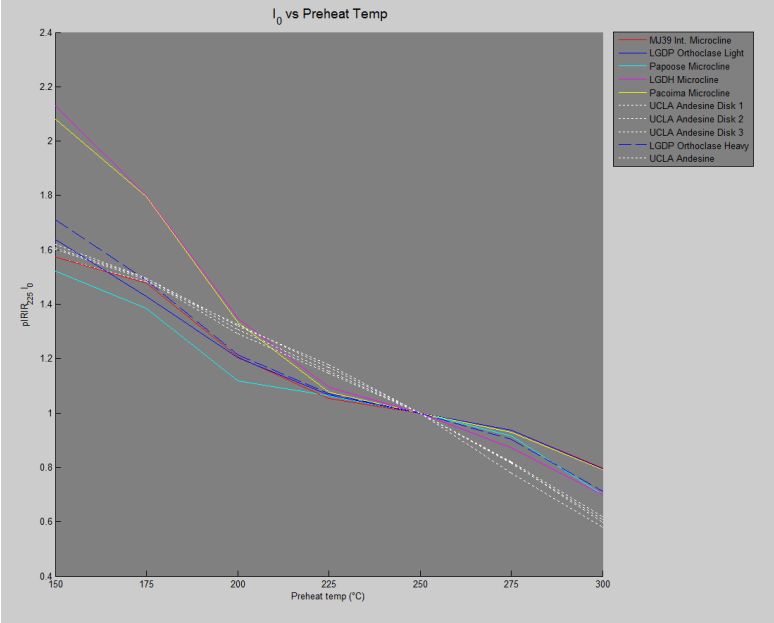

Figure 13 Experiment 1, varying preheat temperature (PH). PH vs. I_0'; each sample normalized to its I_0'value at PH = 250°C. Same data as Figure 12, but main K-feldspar samples plus 011 Na-plagioclase only.

Figure 13 shows the same plot for just the main K-feldspar group and 011 Na-plagioclase. All four of the 011 Na-plagioclase discs are highly consistent with one another. Compared with the main K-feldspar group, its initial intensity generally varies by similar proportional values, but the curve has a slightly different shape. Also discernible on this figure is that 009L LGDP orthoclase light and 009H heavy are a close match. 009H loses slightly more I'_0 with increasing preheat temperature than does 009L.

Looking at parameter *a* in Figure 14, all the K-feldspars have broadly the same behavior with changing preheat: *a* decreases until around 175-200°C, then increases until around 250-275°C, then starts to decrease again. 009H LGDP orthoclase heavy has slightly higher *a* values than 009L LGDP light, but they are otherwise similar, and noticeably higher than any other sample. The amazonite group generally have lower *a* values than the main K-feldspar group, but follow the same general shape. Sample 010 sanidine *a* values fall within those of the main K-feldspar group. For sample 011 Na-plagioclase, its value also decreases slightly until 200°C, but stays relatively steady at preheats above that. The labradorite *a*

values where PH = 150-225°C decrease over this range and are the lowest of all the samples. As previously noted, there are no coherent decays for the labradorites above PH = 225°C.

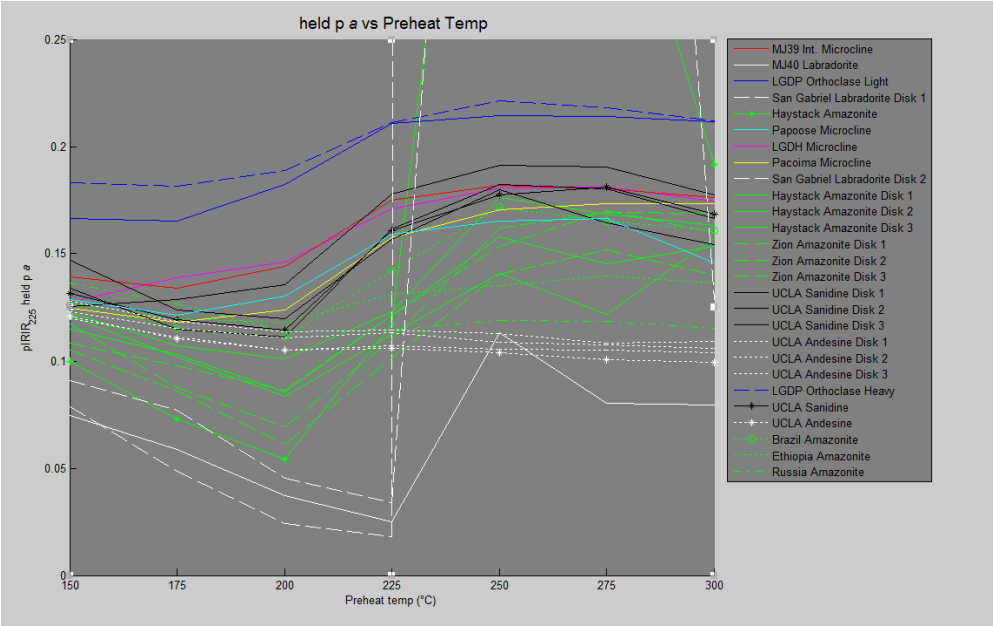

Figure 14 Experiment 1, varying preheat temperature (PH). PH vs. parameter *a*, calculated when *p* is held to 2.

5.2. Second Experiment: pIRIR temperature

The second experiment varied the second IR measurement (the "post-IR-IRSL" or pIRIR) temperature (normally 225°C) from 100-225°C in steps of 25°. The labradorites showed no coherent decay at any of these pIRIR temperatures, and were not analyzed.

Figure 15 shows I'_0 increases monotonically with pIRIR temperature for all samples. Figure 16 normalizes the curves of each sample to their values at $pIRIR_{200}$. The shape of the changing values of I'_0 is very similar within the main K-feldspar group. The shape is somewhat different for sample 011 Na-plagioclase. Sample 010 sanidine plots quite closely with the main K-feldspar group here, which is somewhat surprising given its often distinct behavior in other experiments.

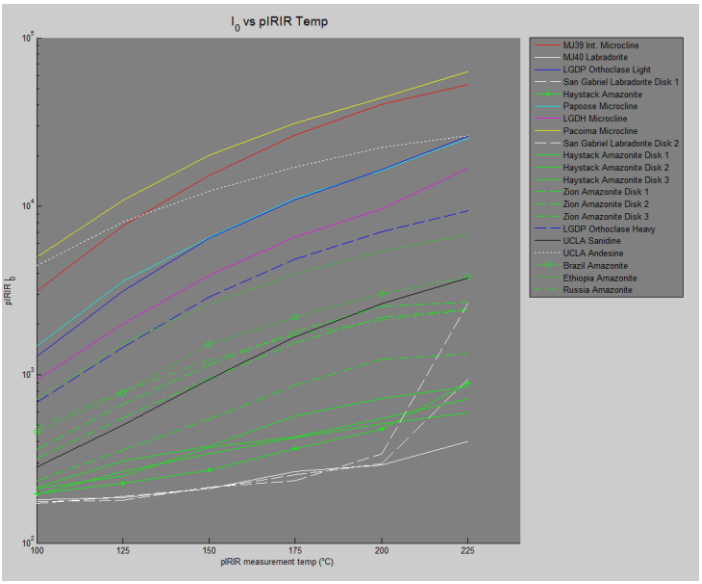

Figure 15 Experiment 2, varying pIRIR measurement temperature ($pIRIR_T$). $pIRIR_T$ vs. initial intensity I_0'. Note log axis.

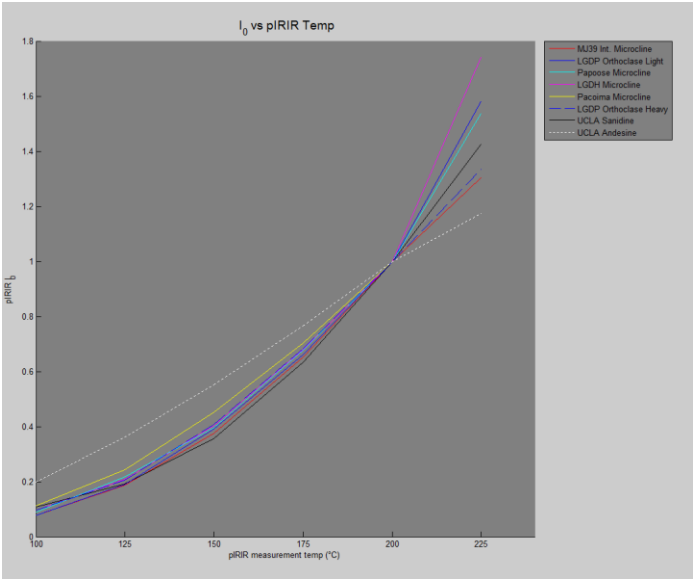

Figure 16 Experiment 2, varying pIRIR measurement temperature ($pIRIR_T$). $pIRIR_T$ vs. initial intensity I_0'; each sample normalized to its I_0' value at $pIRIR_T$ = 200°C.

Parameter *α* increased more or less linearly with pIRIR measurement temperature Figure 17, although the amazonites and especially 003 Haystack discs were a bit noisy. The *α* values for samples 009H and 009L are close to identical to each other for the entire range of pIRIR measurement temperatures. Figure 18, normalized to the value at measurement temperature $pIRIR_{200}$, shows that the main K-feldspar group all plot very closely. Sample 010 sanidine, shows a slight upwards concavity to its plot. 011 Na-plagioclase's shape is also subtly different; it's value of parameter *α* is slightly less sensitive to increases in pIRIR measurement temperature, and its curve has a slightly downward concavity. A slightly better fit is achieved when *p* is allowed to vary; the best fit is calculated with *p* = 1.14 at $pIRIR_{125}$, 1.67 at $pIRIR_{200}$, and 2.05 at $pIRIR_{225}$ (see the Experiment 2 pIRIR Temp Calculated Parameters spreadsheet in supplementary materials). This may be significant; in most of the well-behaved K-feldspar decay fits where *p* is allowed to vary, it rises above 2.

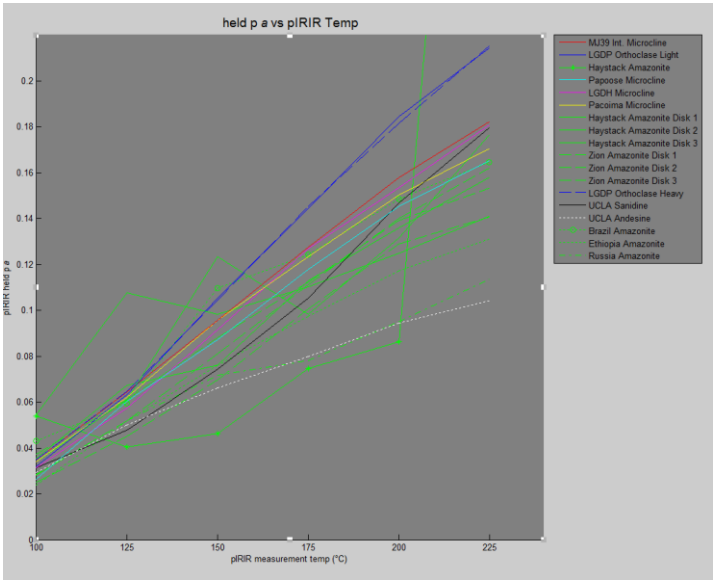

Figure 17 Experiment 2, varying pIRIR measurement temperature ($pIRIR_T$). $pIRIR_T$ vs. parameter *α*, calculated when *p* is held to 2.

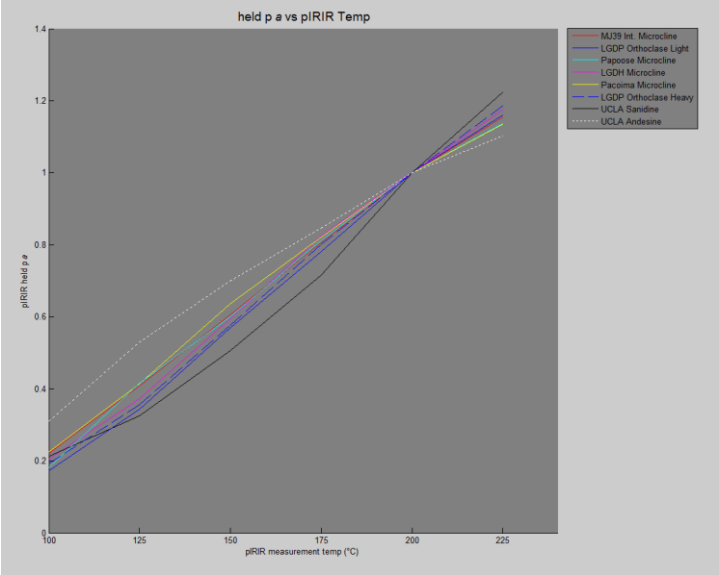

Figure 18 Experiment 2, varying pIRIR measurement temperature ($pIRIR_T$). $pIRIR_T$ vs. parameter *a* (calculated when *p* is held to 2); each sample normalized to its value of a at $pIRIR_T$ = 200°C.

5.3. Third Experiment: First IR time

The third experiment varied the measurement time of the first IR measurement (normally 100 s) from 0.25 to 300 seconds in roughly half order of magnitude steps (0.25, 1, 3, 10, 30, 100, and 300 seconds). Unlike the other experiments, the protocol variable (IR_{50} time) was plotted on a log axis. Labradorites have coherent decays when IR_{50} measurement time is 30 seconds or less.

None of the samples have excellent fits at low IR_{50} times. While the decays are coherent, samples 013 Ethiopia amazonite, 011 Na-plagioclase, 005 LGDH microcline, and 009H LGDP orthoclase heavy can't be said to have valid fits until after IR_{50} times of 10 – 30 seconds. For samples 004 Papoose microcline, 006 Pacoima microcline, 009L LGDP orthoclase light, and 007 MJ39 intermediate microcline, this doesn't happen until IR_{50} times of 30 – 100 seconds. For both of these populations, the calculated fit where *p* is held to 2 systematically overestimates, then underestimates the actual data (Figure 19). Allowing *p* to

vary gives only marginally better fits, often with extreme values of *p*, such as 18. It is more likely that another type of decay is dominant for the $pIRIR_{225}$ signal when IR_{50} time is low.

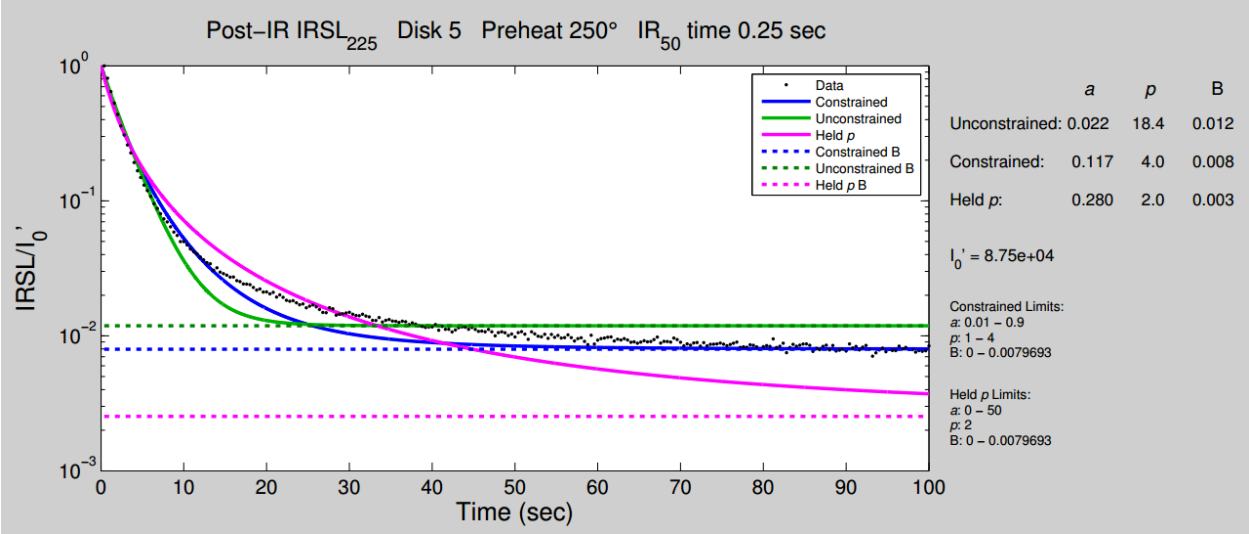

Figure 19 $pIRIR_{225}$ measurement of sample 004 Papoose microcline at IR_{50} time = 0.25 sec. Coherent decay not well fitted by Equation 12.

Labradorites have coherent decays when IR_{50} measurement time is 30 seconds or less.

Brightnesses decrease monotonically for all samples as a function of increasing IR_{50} measurement time (Figure 20). Sample 011 Na-plagioclase is the second brightest at IR_{50} measurement time of 0.25 seconds but drops to third (below sample 007 MJ39 intermediate microcline) between 3 and 10 sec. Sample 006 Pacoima microcline starts out as the brightest sample but drops to slightly below 007 MJ39 right before 100 sec.

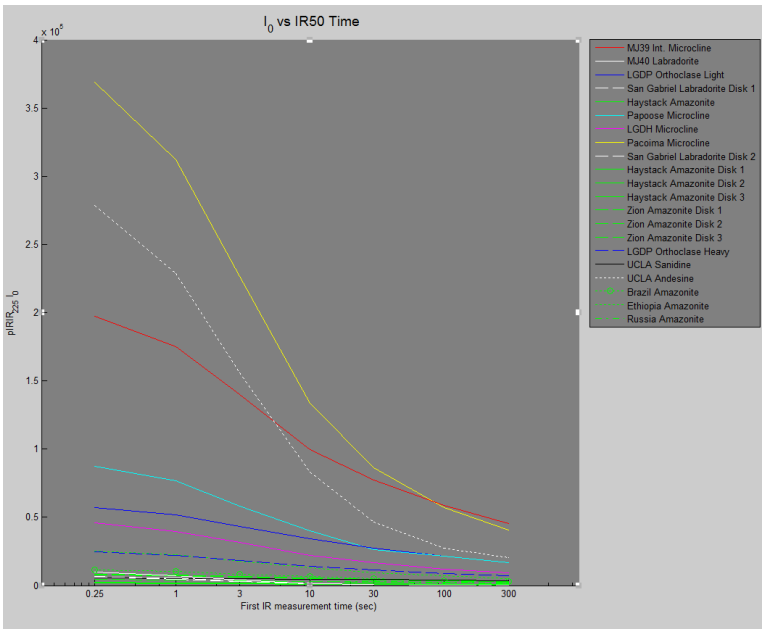

Figure 20 Experiment 3, varying IR_{50} measurement time. IR_{50} time vs. initial intensity I_0'. Note log axis.

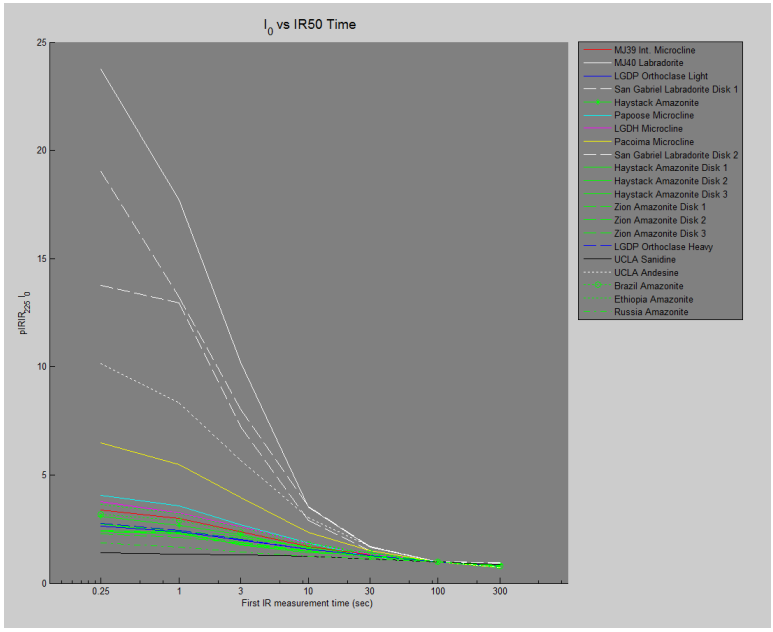

Figure 21 Experiment 3, varying IR_{50} measurement time. IR_{50} time vs. initial intensity I_0', each sample normalized to its I_0' value at IR_{50} time = 100 sec.

Figure 21 normalizes the initial intensity of each sample to that of its value at an IR_{50} measurement time of 100 seconds. The I_0' values of the labradorites are the most sensitive increasing IR_{50} measurement time, followed by sample 011 Na-plagioclase. Sample 006 Pacoima is the most sensitive of all the K-feldspars. 010 sanidine is the least sensitive of any sample, with its brightness nearly unchanging in response to IR_{50} measurement time. The 009 LGDP orthoclase light and heavy samples have very similar curves, with 009H heavy being slightly more sensitive.

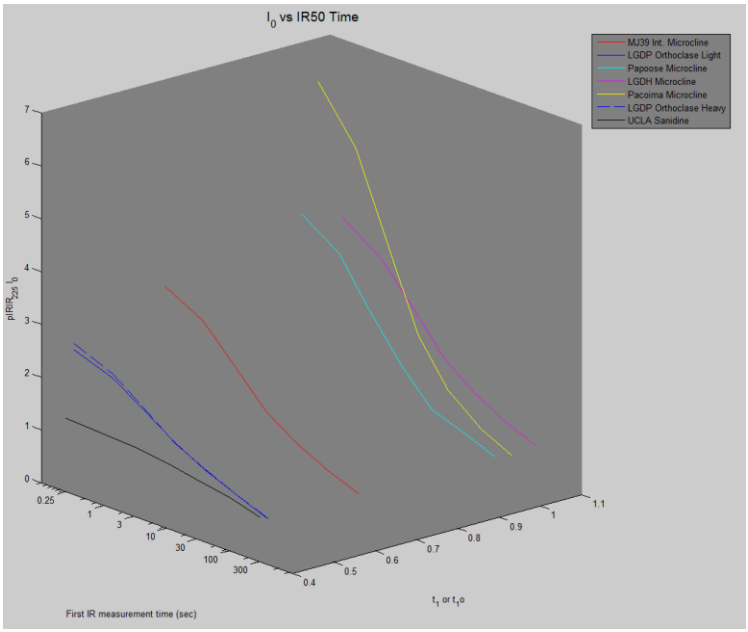

Figure 22 Experiment 3, varying IR_{50} measurement time. IR_{50} time vs. initial intensity I_0', each sample normalized to its I_0' value at IR_{50} time = 100 sec. Z-axis is t_1o (t_1 for monoclinic samples 010 sanidine and 009 LGDP orthoclases). Larger t_1o values indicate higher Al,Si order.

There is a possible positive correlation of increasing I'_0 sensitivity to IR_{50} time with Al,Si ordering (Figure 22); of the main K-feldspar group plus 010 sanidine, 005 LGDH microcline is the only sample that doesn't follow this trend.

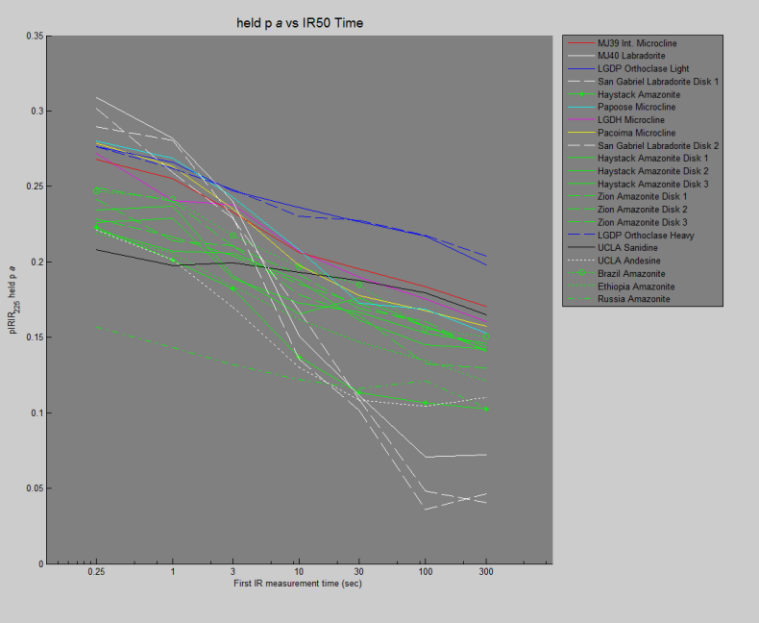

Figure 23 Experiment 3, varying IR_{50} measurement time. IR_{50} time vs. parameter *a* (calculated when *p* is held to 2).

Figure 23 shows a general decreasing trend of parameter *a* with IR_{50} time. Samples 009 LGDP heavy and light are very similar throughout. When the *a* curves are normalized to IR_{50} time = 100 sec, there appears to be a positive correlation between t_1o and *a* for the non-amazonite K-feldspars; that is, increasing Al,Si order seems to be correlated with an increase in the sensitivity of parameter *a* to IR_{50} measurement time (Figure 24). As is typical, sample 005 LGDH microcline is the only sample to not follow this trend; however, the difference here is not as dramatic as other measurements.

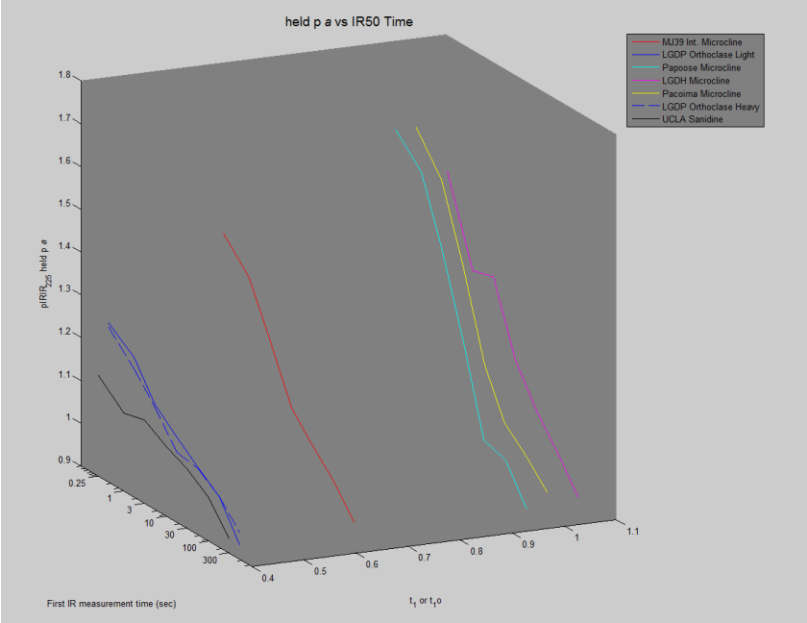

Figure 24 Experiment 3, varying IR_{50} measurement time. IR_{50} time vs. parameter *a* (calculated when *p* is held to 2), each sample normalized to its a value at IR_{50} time = 100 sec. Z-axis is t_1o (t_1 for monoclinic samples 010 sanidine and 009 LGDP orthoclases). Larger t_1o values indicate higher Al,Si order.

5.4. Fourth Experiment: First IR measurement temperature

The fourth experiment varied the temperature of the first IR measurement (normally 50°C and thus called "IR_{50}") from 50-225°C in steps of 25° but kept the duration at 100 sec. As with the other experiments, the decay being analyzed is that of the second IR measurement, $pIRIR_{225}$.

Labradorites do not show clear-cut coherent decay at any value, and are not included in the analysis. The amazonite group is well behaved at low IR measurement temperatures, but at and above 175-200°C, the decay is no longer coherent . 010 sanidine and 009H LGDP orthoclase heavy show the same behavior, except around 200- 225°C. The other K-feldspars and 011 Na-plagioclase have marginally coherent fits at 225°C.

$pIRIR_{225}$ initial intensity I_0' decreases more or less exponentially with increasing IR measurement temperature (Figure 25). Sample 007 MJ39 intermediate microcline is the brightest followed closely by 006 Pacoima microcline. The next brightest is 011 Na-plagioclase. 009H LGDP orthoclase heavy has the lowest I_0' values of the main K-feldspar group.

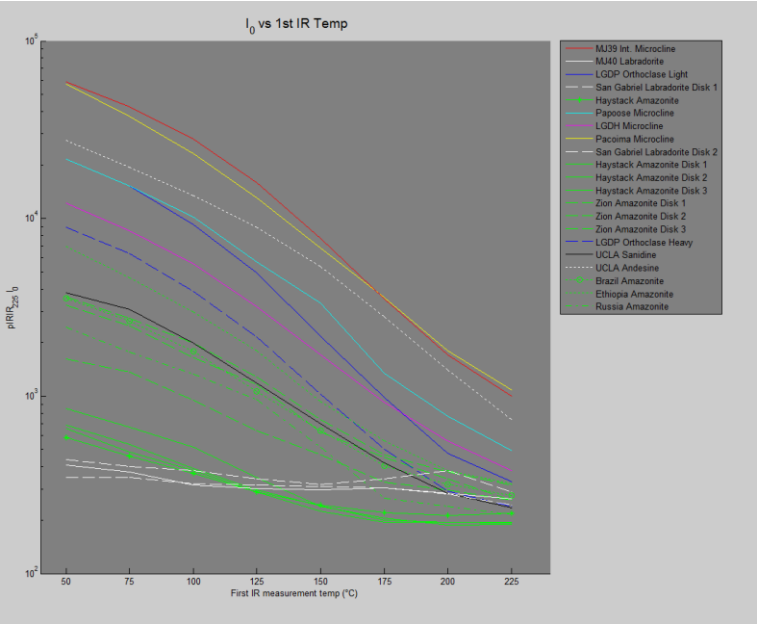

Figure 25 Experiment 4, varying 1st IR measurement temperature (IR_T). IR_T vs. initial intensity I_0'. Note log axis.

The I_0'curves of the main K-feldspar group plus 010 sanidine and 011 Na-plagioclase, when normalized to their values at IR_{50}, are remarkably similar (Figure 26). The sensitivity of the initial intensity of the samples to changing IR measurement temperatures seem to be close to invariant for this group of feldspars.

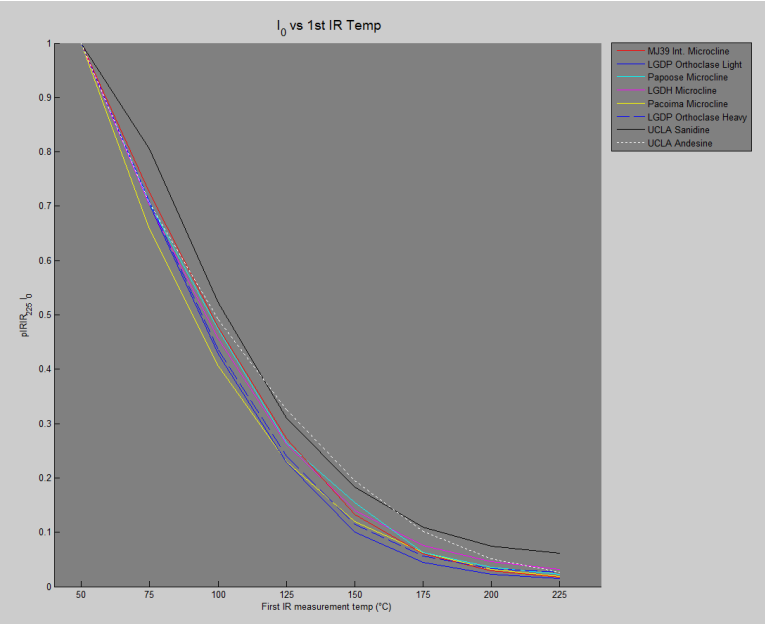

Figure 26 Experiment 4, varying 1st IR measurement temperature (IR_T). IR_T vs. initial intensity I_0', each sample normalized to its I_0' value at IR_T = 50°C.

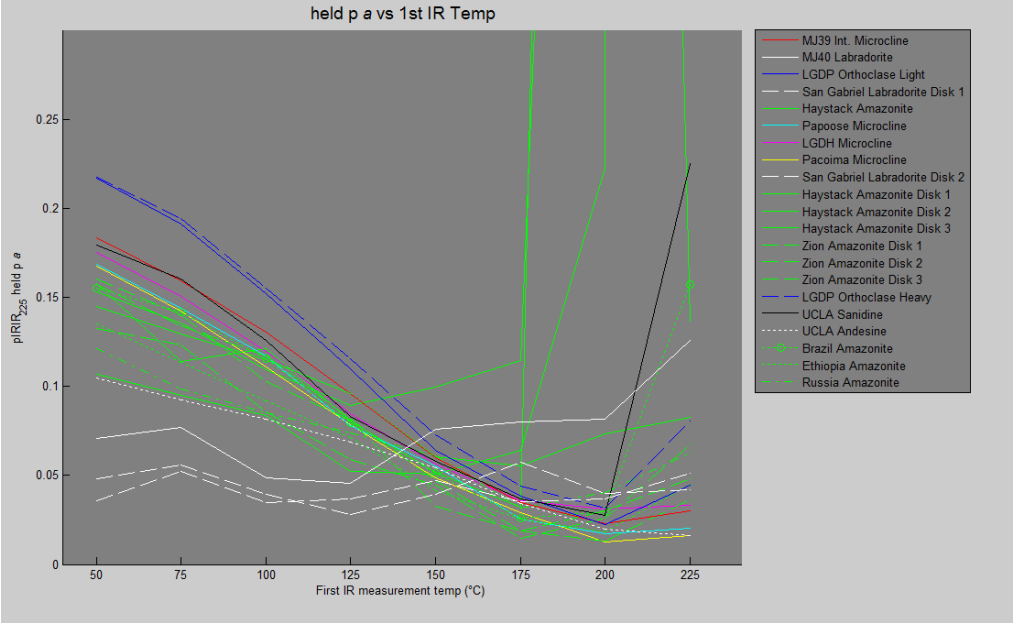

Figure 27 Experiment 4, varying 1st IR measurement temperature (IR_T). IR_T vs. parameter *a* (calculated when *p* is held to 2).

Parameter *a* decreases with increasing IR measurement temperature for most samples up to 200°C, after which it increases slightly in most samples (Figure 27). This behavior occurs at a lower temperature in the amazonites. These increases generally occur at the point where a sample's decay is no longer coherent and *a* starts to lose meaning. Ignoring the amazonite group, sample 009 LGDP orthoclase has the highest *a* values. Na-plagioclase is the lowest. Sample 010 sanidine plots with the main K-feldspar group. When normalized to its value at IR_{50}, the parameter *a* of the non-amazonitic K-feldspars plot closely at IR measurement values below 200°C (Figure 28). The large increase in 010 sanidine is due to the signal becoming incoherent. The difference in parameter *a* sensitivity to changes in protocol parameters of sample 011 Na-plagioclase is more apparent in this experiment; it decreases less quickly than other samples .

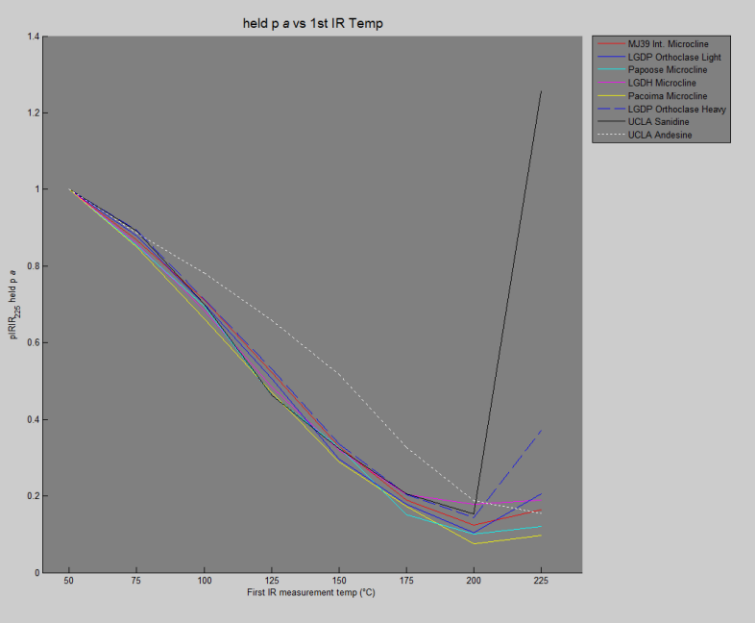

Figure 28 Experiment 4, varying 1st IR measurement temperature (IR_T). IR_T vs. parameter *a* (calculated when *p* is held to 2), each sample normalized to its a value at IR_T = 50°C.

6. Discussion

6.1. Dating implications

The labradorites (calcic plagioclases) do not have a useful decay for currently used pIRIR dating protocols. In the third experiment (varying IR_{50} time), fitting to Equation 12 increases with time but I_0' decreases. An IR_{50} time of 30 seconds (normally it is 100 sec) appears to be the best compromise of clear decay that is still well fitted by Equation 12. This may be a trade-off: a less stable charge is being measured, but we may be able to date feldspars that are usually undatable in situations where no better candidates (quartz or K-feldspar) exist. In the first experiment (varying preheat temperature) , decays disappear around PH = 225°C; as pIRIR measurement temperature is also 225°, it can be assumed there is no thermally stable (needs both optical and thermal stimulation to be liberated) signal at this temperature. Preheats are slightly above pIRIR measurement temperatures to make sure the measured signals are thermally stable. It is possible with both lower preheat and measurement temperatures (PH = 200 for $pIRIR_{175}$, for example) there may be a less theoretically ideal, but realistically accessible, datable signal.

Sample 011 Na-plagioclase does not suffer from dimness/loss of coherent signal like the labradorites, however subtle differences in behavior suggest possibly different charge population distribution and/or electron-hole recombination processes. Comparison with D_e and tests of anomalous fading for this sample are warranted.

Sample 010 sanidine suffered from low signal brightness. In addition, while its luminescence parameters were often worse than the main K-feldspar group, their behavior with varying measurement protocols generally followed the same trends. To find an improved signal for sanidines likely will involve varying

other parameters than studied in this research. While amazonite also suffered from low brightness, its characteristics were more varied, and amazonite is unlikely to be a major component of dated sediments.

For sample 009 LGHP orthoclase, the light portion generally had better luminescence characteristics for dating over the heavy portion, though the effect was small. Further investigation on the effects of SuK on a wider range of feldspar samples is warranted; however, it may be that the dramatic improvement sometimes seen with SuK (such as Rhodes, 2015) is due to the preferential selection of grains of a specific provenance with better dating properties for reasons other than K-content in sediments with multiple parent bodies.

6.2. General behavior observations

All amazonites are dimmer than main K-feldspar group; something other than K-content and Al,Si ordering seems to be interfering with their luminescence. In addition, decays are generally slower (lower *a*). It may possibly be due to the effect of Pb or introduced defect □ on *T*-O bond lengths, though no such measurement of the <<*T*-O>> of amazonites is forthcoming in the literature. The uncertain origin of the color in amazonites further clouds the issue. A more detailed characterization of the minor impurities of the amazonite samples in this thesis is warranted.

Sanidine is dimmer than the main K-feldspar group. While small changes in Al,Si ordering (such as intermediate vs. maximum microclines; sample 007 MJ39 intermediate microcline is the second brightest overall, more than most max microclines) may not cause noticeable changes in behavior, large differences (such as between sanidine and microcline) may. In the main K-feldspar group, 009H LGDP

orthoclase heavy was always second dimmest, and 009L LGDP light fourth. The sample in between, 005 LGDH microcline, is suspected to possibly have not been characterized correctly as it defies several other apparent correlations. While sanidines have been previously established as not ideal for dating (Visocekas & Zink, 1995) It is possible sample 010 dimmer for other reasons, such as its measurable phosphorus content. Analysis of several more sanidine samples in a wider variety of compositions is warranted for confirmation of these results. Tests of analbite (sodic disordered Na-feldspar), compared to more mundane highly-ordered albite, should give more information on Al,Si ordering controls of feldspar luminescence in general.

The normalized luminescence parameters varied the least in the main K-feldspar group in the second and fourth experiments: even for 010 sanidine and (to a lesser extent) 011 Na-plagioclase, the sensitivity of brightness and decay rate to both first IR and pIRIR measurement temperatures were very similar. Samples with higher Al,Si order showed the greatest sensitivity (in both I_0' and a) to IR_{50} measurement time. The differences in sensitivities for varying preheat temperatures is less clear.

Within the main K-feldspar group, there did not appear to be strong controls of Ks content on luminescence characteristics. However, other than density-separated 009H LGDP orthoclase heavy, within this group Ks did not vary by more than 6 mol% (Table 2). An analysis of a true albite, along with alkali feldspars of intermediate composition and very potassic non-amazonitic feldspars, would give more significant results. The data seems to suggest there is some control of Ks content on luminescence characteristics, but the effect is likely mask by other stronger effects such as Al,Si ordering, minor impurities, or other undiscovered factors.

The difference of 011 Na-plagioclase luminescence characteristics from those of the labradorites, and superficial resemblance to the main K-feldspar group, including its high brightness, was initially

surprising, as it has a not insignificant amount of Ca. It is possible its behavior follows the same model as the labradorite decays, which were often too dim or noisy to accurately analyze. Confirmation with other plagioclase samples around An_{30} is warranted, as well as exploring the series between An_{30} and An_{68} to see if there is gradual change in the properties. The composition of 011 Na-plagioclase is at the sodic end of the occurrence of 'e' plagioclase (discussed in section 2.1.2), so albite structure (and ordering) would dominate over that of anorthite.

6.3. First Experiment: Preheat temperature

The labradorites both exhibited weaker and weaker response with increasing preheat temperature, and became incoherent at preheats exceeding 225°C. This may indicate that the labradorite traps are less thermally stable than those of the other feldspars; there may be few to no datable traps that are thermally stable but optically sensitive at 225°C.

Initial IRSL intensity I'_0 decreases more or less monotonically with increasing preheat (PH) for all samples. The more well-behaved samples seem to have an exponential relationship with preheat. Perhaps this indicates that the proportion of thermally stable traps decreases exponentially with increasing temperature. As I_0' drops proportionally faster with increasing preheat temperatures for sanidine and amazonites compared to the main K-feldspar group, this may indicate a greater proportion of traps in amazonites and sanidines are thermally unstable.

Compared with the main K-feldspar group, sample 011 Na-plagioclase's initial intensity generally varies by similar proportional values, but the curve has a slightly different shape. There may be a difference in the law (or some constant consistent in the main K-feldspar group) concerning trap thermal stability in sodic plagioclases.

Looking at *a*, all the K-feldspars have broadly the same behavior: it decreases until around 175-200°C, then increases until around 250-275°C, then starts to decrease again. As higher *a* indicates a more bleachable signal better for dating (to a point), it seems that PH = 250°C is confirmed as a good choice for $pIRIR_{225}$. For sample 011 Na-plagioclase, *a* also decreases slightly until 200°C, but stays relatively steady after this. It is clear that the signal of Na-plagioclase is fundamentally different – there may be differences in the connectivity or nature of the band-tail states or "internal plumbing" as discussed in section 2.2. Perhaps the thermal stability of traps is less impactful for Na-plagioclase luminescence.

6.4. Second Experiment: pIRIR temperature

The proportional change in I_0'and *a* with preheat temperature was very similar in not only the main K-feldspar group, but also 010 sanidine as well, indicating invariance with different amounts of Al,Si disorder. Once again, there are differences in 011 Na-plagioclase behavior of luminescence characteristics with protocol variables, although they are much more subtle here. Its initial intensity I_0' seems to be slightly less sensitive to change in pIRIR measurement temperature in Na-plagioclase. The possible increase of *p* with pIRIR measurement temperature in this sample could indicate increase of kinetic order at higher temperatures. The almost identical absolute values of a for both 009 LGDP orthoclase light and heavy indicate that small changes in Ks may not affect decay rate at the standard dating protocol values of preheat temperature and IR_{50} measurement time and temperature.

6.5. Third Experiment: First IR time

Unlike the other experiments, this set of protocol variables is significant in that it was the only one to give coherent decays NOT well-fitted with Equation 12. No samples fit well at IR_{50} time = 0.25 seconds,

but the samples that required higher IR_{50} times for a good fit tended to be those with better overall dating characteristics, high I_0' in particular.

It is possible that the signal that would otherwise be released at longer times of IR_{50} is luminescing instead during the $pIRIR_{225}$ measurement, perhaps with that population decaying following a different equation (additive to the standard $pIRIR_{225}$ signal), or with the same equation but different parameters *a* or *p* giving a faster decay. Parameter *a* dropping more with the affected feldspars (which may be linked to Al,Si ordering in the main K-feldspar group) lends credence to this theory –leftover signal from short IR_{50} times would give a rapid decay at the start of the $pIRIR_{225}$ measurement time but drop off quickly.

The samples more affected by this "fit mismatch" would theoretically have a bigger difference in the nature/behavior of the charge populations accessed by IR_{50} vs $pIRIR_{225}$. If the charge populations had the same fundamental recombination behavior, a single equation would be sufficient to fit the decay. If charge populations have the same recombination behavior, they are more likely to be stimulated by similar conditions, which means there would be less of a stable signal available at $pIRIR_{225}$ – indeed, dimmer samples tended to reach an acceptable fit to Equation 12 better at lower IR_{50} measurement times: the labradorites have no $pIRIR_{225}$ signal at all at IR_{50} times past 30 seconds.

6.6. Fourth Experiment: First IR temperature

The result of the fourth experiment was very similar to those of the second (pIRIR temperature). All of the main K-feldspars plus 010 sanidine showed very similar sensitivities of I_0' and *a* to changes in IR and pIRIR measurement temperatures, with 011 Na-plagioclase showing subtle variations. While the absolute brightness may vary between K-feldspars, this suggests that the recombination behavior of

thermally stable signals is invariant to Al,Si order and to a certain extent major composition , though amazonites showed considerably greater variation in both experiments.

7. Conclusion

In the course of this study, the possibility that the length (or possibly angle) of the *T*-O bonds is the main factor affecting luminescence behavior in all feldspars became apparent. The tectosilicate structure seems to be important to luminescence – it is shared by both quartz and feldspar, along with feldspathoids such as leucite, which have also been found to have IRSL signals (Tsukamoto et al., 2014). Poolton et al. (2002b) suggested that the varying lengths or angles of the *T*-O bond in feldspars, due to complications of Al^{3+} effect on bond length, was the critical factor in the creation of the non-quantized band-tail states, which are not found in the more structurally uniform quartz (discussed in Section 2.1.2.1 and 2.2.2).

The average *T*-O bond length <<*T*-O>> in quartz is 1.60-1.61 (Å), and changes of as little as 0.1 (Å) can change the band gap depth by 3.5 eV; << *T*-O>> of albite is 1.64; anorthite is 1.68. The band gap depth in feldspars is around 7.7 eV (Jain & Ankjærgaard, 2011). If the lengths of bonds in feldspar are sensitive to changes in a similar fashion to quartz, it seems that the dimness and poor dating characteristics of calcic plagioclases arise not from the Ca content, but the increased Al content: the <<*T*-O>> increases until charge can no longer bridge the gap.

As Si-O bond lengths are 0.03 longer if O is coordinated to another Si than Al, ordering may change the variation and distribution of bond lengths in the crystal. The large cations also change bond lengths, though to a lesser extent than Al,Si ordering. This could explain why there is still a difference between the behavior of potassic and sodic feldspars, but the difference is not as great as the more aluminous

calcic feldspars. It may also play a role in the anomalous character of the amazonites, though it is unclear how such low concentrations of Pb or structural water could have such a large effect.

Variations in *T*-O bond length may explain everything from the lack of sensitivity in calcic plagioclases to the differences in behavior of disordered sanidine, and possibly the anomalous luminescence properties of amazonites. All of the observed mineralogic controls on luminescence behavior affect (or are affected by) *T*-O bond length.

References

Angel, R. J., & Finger, L. W. (1990). Structural variation associated with compositional variation and order-disorder behavior in anorthite-rich feldspars. American Mineralogist, 7(5), 150-162.

Aitken, M. J. (1998). An introduction to optical dating: the dating of Quaternary sediments by the use of photon-stimulated luminescence. Oxford University Press.

Amiotte Suchet, P., Probst, J. L., & Ludwig, W. (2003). Worldwide distribution of continental rock lithology: Implications for the atmospheric/soil CO2 uptake by continental weathering and alkalinity river transport to the oceans. Global Biogeochemical Cycles, 17(2).

Auclair, M., Lamothe, M., and Huot, S. (2003) Measurement of anomalous fading for feldspar IRSL using SAR. Radiation Measurements. 37, 487–492. doi: 10.1016/s1350-4487(03)00018-0

Bailey, R. M. (2004). Paper I—simulation of dose absorption in quartz over geological timescales and its implications for the precision and accuracy of optical dating. Radiation Measurements, 38(3), 299-310.

Bailiff, I. K., & Barnett, S. M. (1994). Characteristics of infrared-stimulated luminescence from a feldspar at low temperatures. Radiation Measurements,23(2-3), 541-545.

Brill, D., Klasen, N., Brückner, H., Jankaew, K., Scheffers, A., Kelletat, D., & Scheffers, S. (2012). OSL dating of tsunami deposits from Phra Thong Island, Thailand. Quaternary Geochronology. 10, 224-229.

Brown, N. D., Rhodes, E. J., Antinao, J. L., & McDonald, E. V. (2015). Single-grain post-IR IRSL signals of K-feldspars from alluvial fan deposits in Baja California Sur, Mexico. Quaternary International, 362, 132-138.

Buylaert, J. P., Jain, M., Murray, A. S., Thomsen, K. J., Thiel, C., & Sohbati, R. (2012). A robust feldspar luminescence dating method for Middle and Late Pleistocene sediments. Boreas, 41(3), 435-451.

Buylaert, J. P., Murray, A. S., Thomsen, K. J., & Jain, M. (2009). Testing the potential of an elevated temperature IRSL signal from K-feldspar. Radiation Measurements, 44(5), 560-565.

Carter, B. A. (1982). Field petrology and structural development of the San Gabriel anorthosite-syenite body, Los Angeles County, California. Geologic Excursion jn the Transverse Ranges, edited by JD Cooper, pp. J-47, Geological Society of America, Boulder, Colo.

Carter, B.A. (1980). Geology of the anorthosite-syenite terrain, San Gabriel Mountains, Los Angeles County, California.[Map]. ca. 1:30,000. PhD thesis, California Institute of Technology, Pasadena, California.

Čech, F., Mísař, Z., & Povondra, P. (1971). A green lead-containing orthoclase. Tschermaks mineralogische und petrographische Mitteilungen,15(3), 213-231.

Deer, W. A., Howie, R. A., & Zussman, J. (Eds.). (2001). Rock-forming Minerals: Feldspars, Volume 4A. Geological Society of London.

Dibblee, T.W., and Ehrenspeck, H.E. (2001). Geologic map of the Pacifico Mountain and Palmdale (south half) quadrangles, Los Angeles County, California: Dibblee Geological Foundation, Dibblee Foundation Map DF-76, scale 1:24,000

Dibblee, T.W., and Ehrenspeck, H.E., ed. (1991). Geologic map of the Sunland and Burbank (north 1/2) quadrangles, Los Angeles County, California: Dibblee Geological Foundation, Dibblee Foundation Map DF-32, scale 1:24,000

Dibblee, T.W., and Minch, J.A. (2002). Geologic map of the Chilao Flat quadrangle, County, California: Dibblee Geological Foundation, Dibblee Foundation Map DF-85, scale 1:24,000

Duller, G. A. T. (1997). Behavioural studies of stimulated luminescence from feldspars. Radiation Measurements, 27(5), 663-694.

Egerton, R. F. (2005). Physical Principles of Electron Microscopy: An Introduction to TEM, SEM, and AEM.

Ehlig, P. L. (1981). Origin and tectonic history of the basement terrane of the San Gabriel Mountains, central Transverse Ranges. The geotectonic development of California, 1, 253-283.

Fattahi, M., & Stokes, S. (2003). Dating volcanic and related sediments by luminescence methods: a review. Earth-Science Reviews, 62(3), 229-264.

Foord, E. E., & Martin, R. F. (1979). Amazonite from the Pikes Peak batholith. Mineralogical Record, 10(6), 373-84.

Graham, D., and Midgley, N. (2000). Triangular diagram plotting spreadsheet (TRI-PLOT) [computer program]. Version 1.4. Loughborough, England. Loughborough University.

Griffis, R. A. (1987). Kern knob pluton and other highly-evolved granitoids in East-central California.

Hofmeister, A. M., & Rossman, G. R. (1985). A spectroscopic study of irradiation coloring of amazonite: structurally hydrous, Pb-bearing feldspar.American Mineralogist, 70(7-8), 794-804.

Huntley, D.J., and Lamothe, M. (2001) Ubiquity of anomalous fading in K-feldspars and the measurement and correction for it in optical dating. Canadian Journal of Earth Sciences. 38, 1093 -1106. doi: 10.1139/cjes-38-7-1093

Itoh, N., Stoneham, D., & Stoneham, A. M. (2002) Ionic and electronic processes in quartz: mechanisms of thermoluminescence and optically stimulated luminescence. Journal of Applied Physics. 92(9), 5036-5044.

Jain, M., & Ankjærgaard, C. (2011). Towards a non-fading signal in feldspar: insight into charge transport and tunnelling from time-resolved optically stimulated luminescence. Radiation Measurements, 46(3), 292-309.

Jain, M., Sohbati, R., Guralnik, B., Murray, A. S., Kook, M., Lapp, T., ... & Buylaert, J. P. (2015). Kinetics of infrared stimulated luminescence from feldspars. Radiation Measurements, 81, 242-250.

Krbetschek, M. R., Götze, J., Dietrich, A., & Trautmann, T. (1997). Spectral information from minerals relevant for luminescence dating. Radiation Measurements, 27(5), 695-748.

Kroll, H., & Ribbe, P. H. (1983) Lattice parameters, composition and Al, Si order in alkali feldspars. Reviews in Mineralogy. 2, 57-99.

Kuehner, S. M., & Joswiak, D. J. (1996). Naturally occurring ferric iron sanidine from the Leucite Hills lamproite. American Mineralogist, 81(1-2), 229-237.

Lamothe, M., Auclair, M., Hamzaoui, C., & Huot, S. (2003). Towards a prediction of long-term anomalous fading of feldspar IRSL. Radiation Measurements, 37(4), 493-498.

Lawson, M. J., Daniels, J. T., & Rhodes, E. J. (2015). Assessing Optically Stimulated Luminescence (OSL) signal contamination within small aliquots and single grain measurements utilizing the composition test. Quaternary International, 362, 34-41.

Le Bas, M. J., & Streckeisen, A. L. (1991). The IUGS systematics of igneous rocks. Journal of the Geological Society, 148(5), 825-833.

Li, Y. P., & Ching, W. Y. (1985). Band structures of all polycrystalline forms of silicon dioxide. Physical Review B, 31(4), 2172.

McGuire, C., & Rhodes, E. J. (2015). Determining fluvial sediment virtual velocity on the Mojave River using K-feldspar IRSL: Initial assessment.Quaternary International, 362, 124-131

Melluso, L., Morra, V., & Di Girolamo, P. (1996). The Mt. Vulture volcanic complex (Italy): evidence for distinct parental magmas and for residual melts with melilite. Mineralogy and Petrology, 56(3-4), 225-250.

Miller, W. J. (1936). Geology of the Western San Gabriel Mountains of California.

Morthekai, P., Jain, M., Gach, G., Elema, D. R., & Prip, H. (2013). Dependence of (anomalous) fading of infra-red stimulated luminescence on trap occupancy in feldspars. Journal of Luminescence, 143, 704-709.

Murray, A.S. & Olley, J. M. (2002) Precision and accuracy in the optically stimulated luminescence dating of sedimentary quartz: A status review. Geochronometria. 21, 1-16 .

Nelson, C.A. (1966). Geologic Map of Waucoba Mountain quadrangle, Inyo Country, California [Map]. 1:62,500. US Geological Survey.

Nesse, W.D. (2012) Introduction to Mineralogy, Second Edition. Oxford University Press, Oxford, UK.

Neuerburg, G. J. (1954). ALLANITE PEGMATITE, SAN GABRIEL MOUNTAINS, LOS-ANGELES COUNTY, CALIFORNIA. American Mineralogist, 39(9-10), 831-834.

Nickel, E. H. (1992). Solid solutions in mineral nomenclature. Mineralogy and Petrology, 46(1), 49-53.

Pecharsky, V. K., & Zavalij, P. Y. (2009). Fundamentals of powder diffraction and structural characterization of materials (Vol. 69). New York: Springer.

Pettijohn, F. J., Potter, P. E., & Siever, R. (1987). Sand and Sandstone. Springer Science & Business Media. 36.

Poolton, N. R. J., Kars, R. H., Wallinga, J., & Bos, A. J. J. (2009). Direct evidence for the participation of band-tails and excited-state tunnelling in the luminescence of irradiated feldspars. Journal of Physics: Condensed Matter,21(48), 485505.

Poolton, N. R. J., Ozanyan, K. B., Wallinga, J., Murray, A. S., & Bøtter-Jensen, L. (2002). Electrons in feldspar II: a consideration of the influence of conduction band-tail states on luminescence processes. Physics and Chemistry of Minerals, 29(3), 217-225.

Poolton, N. R. J., Wallinga, J., Murray, A. S., Bulur, E., & Bøtter-Jensen, L. (2002). Electrons in feldspar I: on the wavefunction of electrons trapped at simple lattice defects. Physics and Chemistry of Minerals, 29(3), 210-216.

Rhodes, E. J. (2011). Optically stimulated luminescence dating of sediments over the past 200,000 years. Annual Review of Earth and Planetary Sciences, 39, 461-488.

Rhodes, E. J. (2015). Dating sediments using potassium feldspar single-grain IRSL: Initial methodological considerations. Quaternary International, 362, 14-22.

Rhodes, E. J., & Bailey, R. M. (1997). The effect of thermal transfer on the zeroing of the luminescence of quartz from recent glaciofluvial sediments.Quaternary Science Reviews, 16(3), 291-298.

Ribbe, P. H., & Ribbe, P. H. (1983). Feldspar mineralogy (No. 549.6 FEL).

Rupp, B. (2013). Program S E X I E for Reciprocal Cell Spacing [computer program]. Version 5.3. Vista, CA.

Silver, L. T. (1968). Pre-Cretaceous basement rocks and their bearing on large-scale displacements in the San Andreas fault system. Stanford University Publications. Geological Sciences, 11, 279-280.

Silver, L. T. (1971). Problems of crystalline rocks of the Transverse Ranges. In Geological Society of America Abstracts with Programs (Vol. 3, No. 2, pp. 193-194).

Smedley, R. K., Duller, G. A. T., Pearce, N. J. G., & Roberts, H. M. (2012). Determining the K-content of single-grains of feldspar for luminescence dating. Radiation Measurements, 47(9), 790-796.

Smedley, R. K., Duller, G. A. T., & Roberts, H. M. (2015). Bleaching of the post-IR IRSL signal from individual grains of K-feldspar: Implications for single-grain dating. Radiation Measurements, 79, 33-42.

Smith, J. V. (1983). Some chemical properties of feldspars. Mineralogical Society of America Short Course Notes, 2.

Smith, J. V., & Brown, W. L. (1988). Feldspar Minerals. 1 Crystal Structures, Physical, Chemical and Microstructural Properties.

Spooner, N. A. (1992). Optical dating: preliminary results on the anomalous fading of luminescence from feldspars. Quaternary Science Reviews, 11(1), 139-145.

Spooner, N. A. (1993). The validity of optical dating based on feldspar (Doctoral dissertation, University of Oxford).

Spooner, N. A. (1994). The anomalous fading of infrared-stimulated luminescence from feldspars. Radiation Measurements, 23(2), 625-632.

Stevenson, R. K., & Martin, R. F. (1986). Implications of the presence of amazonite in the Broken Hill and Geco metamorphosed sulfide deposits.Can. Mineral, 24, 729-745.

Stokes, S. & Fattahi, M. (2003) Red emission luminescence from quartz and feldspar for dating application: an overview. Radiation Measurements. 37,383-395.

Stone, Paul, Dunne, G.C., Moore, J.G., and Smith, G.I. (2000). Geologic map of the Lone Pine 15' quadrangle, Inyo County, California: U.S. Geological Survey, Geologic Investigations Series Map I-2617, scale 1:62,500

Su, S. C., Ribbe, P. H., Bloss, F. D., & Warner, J. K. (1986). Optical properties of a high albite (analbite)-high sanidine solid-solution series. American Mineralogist, 71(11-12), 1393-1398.

Sylvester, A. G., Ortel, G., Nelson, C. A., & Christie, J. M. (1978). Papoose Flat pluton: A granitic blister in the Inyo Mountains, California. Geological Society of America Bulletin, 89(8), 1205-1219.

Thiel, C., Buylaert, J., Murray, A., Terhorst, B., Hofer, I., Tsukamoto, S., and Frechen, M. (2011) Luminescence dating of the Stratzing loess profile (Austria) – Testing the potential of an elevated temperature post-IR IRSL protocol. Quaternary International, 234(1-2), 23-31.

Thomsen, K.J., Murray, A.S., Jain, M. & Bøtter-Jensen, L., (2008) Laboratory fading rates of various luminescence signals from feldspar- rich sediment extracts. Radiation Measurements. 43, 1474-1486.

Tsukamoto, S., Jain, M., Murray, A., Thiel, C., Schmidt, E., Wacha, L., ... & Frechen, M. (2012). A comparative study of the luminescence characteristics of polymineral fine grains and coarse-grained K-and Na-rich feldspars. Radiation measurements, 47(9), 903-908.

Tsukamoto, S., Kataoka, K., Oguchi, T., Murray, A. S., & Komatsu, G. (2014). Luminescence dating of scoria fall and lahar deposits from Somma–Vesuvius, Italy. Quaternary Geochronology, 20, 39-50.

Visocekas, R., and Zink, A. (1995). Tunneling afterglow and point

defects in feldspars. Radiation Effects and Defects in Solids,

134: 265–272.

Wintle, A.G. (1973) Anomalous fading of thermoluminescence in mineral samples. Nature. 245(5421), 143-144.

Xu, Y. N., & Ching, W. Y. (1991). Electronic and optical properties of all polymorphic forms of silicon dioxide. Physical Review B, 44(20), 11048.